Pierre SOILLE

Morphological Image Analysis.

Principles and Applications.

Second Edition, Springer, Berlin 2004

5. Hit-or-miss and Skeletons

In contrast to morphological transformations described so far, the hit-or-miss transformation involves SEs composed of *two* sets. The first has to fit the object under study while the second has to miss it. Hence, the name *fit-and-miss* would have been more appropriate. Hit-or-miss transformations extract all image pixels satisfying a given neighbourhood configuration such as that corresponding to an isolated background or foreground pixel. Adding to an image all pixels having a given configuration leads to the thickening operator while subtracting them from the image defines the thinning operator.

Sequential iterations of thinnings with specific composite SEs generate a medial axis of the input set. This medial axis will be called skeleton. It consists of a compact representation which preserves only those points of a set whose minimum distance to the boundary of the set reaches at least two distinct boundary points. The skeletal points and their distance to the boundary of the set enable the reconstruction of the set. Applications of skeletons range from shape analysis and pattern recognition to data compression. They are also used to reduce thick objects to one-pixel thick curves that can be further processed. For example, thin lines can be converted into a graph by associating their characteristic points with vertices. The resulting graph is then used as an input to graph matching algorithms, e.g., for character recognition. Thin lines are also required for converting a raster image into a vector representation (this process is called *vectorisation*). Skeletons of grey tone images have found useful applications for the extraction of crest lines appearing in their topographic representation. They are also used for computing Euclidean skeletons of binary images by processing their Euclidean distance transform.

In practice, there exist several types of skeletonisation algorithms, each of them satisfying specific properties. For example, the skeletonisation by influence zones delineates the influence zones of the connected components of object pixels of an image (the influence zone of a connected component of pixels being the set of image pixels that are closer to this component than any other component). Morphological transformations of higher level such as the watershed transformation are based on the notion of influence zones.

The chapter is organised as follows. In Section 5.1, the hit-or-miss transforms is defined and its utility for extracting specific patterns and computing

the connectivity number of an image is highlighted. The related concepts of hit-or-miss opening and rank hit-or-miss are also set forth. Thinnings and thickenings are presented in Secs. 5.2 and 5.3 respectively. Five equivalent definitions of the skeleton of a continuous set are introduced in Sec. 5.4 while their adaptation to the discrete framework is detailed in Sec. 5.5 together with their respective properties and usefulness for solving practical problems. Hints about the computation of hit-or-miss and skeleton transforms are detailed in Sec. 5.6. Finally, bibliographical notes and references are given in Sec. 5.7.

5.1 Hit-or-miss transform

The basic idea behind the hit-or-miss transform consists in extracting all image pixels matched by a given neighbouring configuration such as a foreground pixel surrounded by background pixels, i.e., an isolated foreground pixel. The neighbouring configuration is therefore defined by two disjoint sets, the first for the foreground pixels and the second for the background pixels. These two sets form what we call a composite SE which has a unique origin, i.e., both sets share the same origin. Composite SEs used for extracting isolated pixels are shown in Fig. 5.1 for the hexagonal and square grids.

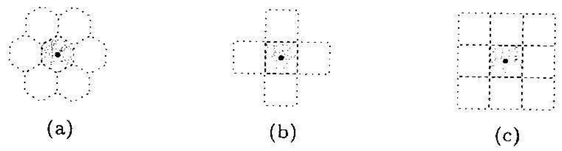

Fig. 5.1. Composite SEs corresponding to the neighbouring configurations of an isolated foreground pixel in the hexagonal (a), 4-connected (b), and 8-connected (c) grids. In this example, the origin of each composite SE is the middle pixel. The white pixels represent the set of background pixels and the grey pixels the set of foreground pixels.

In order to perform a hit-or-miss transform, the SE is set to every possible position of the image. At each position, the following question is considered *"Does the first set* fit *the foreground while, simultaneously, the second set* misses *it (i.e., fits the background)?"* If the answer is affirmative, then the image point matched by the origin of the SE is a point of the hit-or-miss transformation of the image. Let us now formalise this definition in terms of morphological transformations, first concentrating on binary images.

5.1.1 Binary case

A *composite structuring element* contains two structuring elements. The first, denoted by B_{FG}, defines the set of pixels that should match the foreground

while the second, denoted by B_{BG}, defines the set of pixels that should match the background. By definition, B_{FG} and B_{BG} share the *same* origin and are disjoint sets, i.e., $B_{\mathrm{FG}} \cap B_{\mathrm{BG}} = \emptyset$. We use the generic notation $\mathbf{B}$ for a composite SE, i.e., $\mathbf{B} = (B_{\mathrm{FG}}, B_{\mathrm{BG}})$.

The hit-or-miss transformation, HMT, of a set X by a composite structuring element $\mathbf{B} = (B_{\mathrm{FG}}, B_{\mathrm{BG}})$ is the set of points, $\mathbf{x}$, such that when the origin of $\mathbf{B}$ coincides with $\mathbf{x}$, B_{FG} fits X while B_{BG} fits X^c:

$$\mathrm{HMT}_{\mathbf{B}}(X) = \{\mathbf{x} \mid (B_{\mathrm{FG}})_{\mathbf{x}} \subseteq X,\ (B_{\mathrm{BG}})_{\mathbf{x}} \subseteq X^c\}. \tag{5.1}$$

The hit-or-miss transformation of a set X by a composite structuring element $\mathbf{B}$ is sometimes denoted by $X \circledast \mathbf{B}$. Using the definition of the erosion (Eq. 3.1), the HMT can be written in terms of an intersection of two erosions:

$$\mathrm{HMT}_{\mathbf{B}}(X) = \varepsilon_{B_{\mathrm{FG}}}(X) \cap \varepsilon_{B_{\mathrm{BG}}}(X^c). \tag{5.2}$$

Depending on whether the origin belongs to B_{FG} or B_{BG} the HMT extracts foreground or background pixels.

An example is provided in Fig. 5.2. Both SEs of the composite SE $\mathbf{B}$ are discs but they have a common origin located at the centre of the grey disc B_{FG}. It follows that B_{BG} does not contain its origin. Points of the hit-or-miss

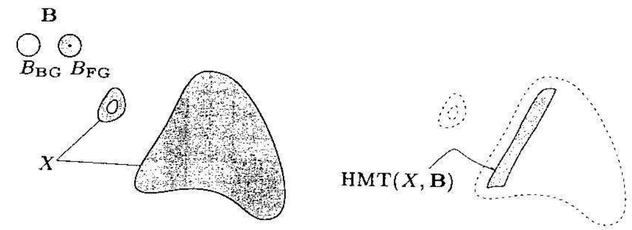

Fig. 5.2. Hit-or-miss transformation HMT of a set X by a composite structuring element $\mathbf{B}$ (B_{FG} is the grey disc and B_{BG} the white disc, the origin of both discs is located at the centre of B_{FG}).

transform of the set X by the composite SE $\mathbf{B}$ (see right side of the figure) are such that when the origin of $\mathbf{B}$ coincides with each of these points, the disc B_{FG} fits X and, simultaneously, the disc B_{BG} fits the background of X. Hence, the hit-or-miss transformation extracts all image points having the same neighbourhood configuration as that defined by the composite SE $\mathbf{B}$.

In the sequel, we denote by $\mathbf{B}^c$ the composite SE with the foreground and background components of $\mathbf{B}$ swapped, i.e., if $\mathbf{B} = (B_1, B_2)$ then $\mathbf{B}^c = (B_2, B_1)$. Consequently, the set of image pixels having B_1 as foreground and B_2 as background neighbourhoods is identical to the set of pixels of the complemented image having B_2 as foreground and B_1 as background neighbourhoods:

$$\mathrm{HMT}_{\mathbf{B}}(X) = \mathrm{HMT}_{\mathbf{B}^c}(X^c).$$

This latter equation reveals that $\mathrm{HMT}_{\mathbf{B}}$ and $\mathrm{HMT}_{\mathbf{B}^c}$ are complementary image transformations (in the sense of Eq. 2.20, page 55): $\mathrm{HMT}_{\mathbf{B}} = \mathrm{HMT}_{\mathbf{B}^c}\complement$.

5.1.2 Grey scale extensions

Equation 5.2 could be extended to grey scale images but in this latter case we would combine the erosion of a grey scale image with an erosion of the complement of this image. Consequently, the result would depend on the value used for complementing the image. In addition, the stacking of the hit-or-miss transformations of the successive cross-sections of a grey scale image does not define the subgraph of a grey scale image because the hit-or-miss is *not* an increasing transformation. Indeed, there may be some t_i such that $\mathrm{HMT}_{\mathbf{B}}[\mathrm{CS}_{t_i}(f)] \not\subseteq \mathrm{HMT}_{\mathbf{B}}[\mathrm{CS}_{t_{i-1}}(f)]$. However, as illustrated in Fig. 5.3 for a 1-D signal, when we position $\mathbf{B}$ at a given pixel $\mathbf{x}$, B_{FG} matches the cross-sections of f from the level 0 up to a given level which we denote by t_{FG}, while B_{BG} matches the complement of the cross-sections of f from the level $t_{\max}+1$ down to a given level which we denote by t_{BG}. For example, in

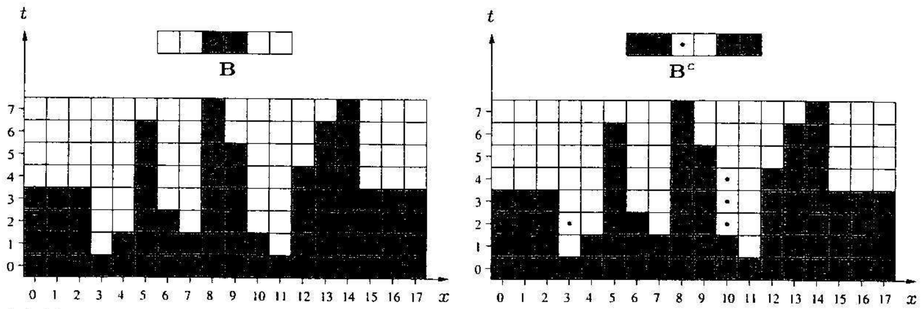

(a) SE $\mathbf{B}$ and input signal f with its subgraph highlighted in grey.

(b) SE $\mathbf{B}^c$ and input signal f with its subgraph highlighted in grey.

Fig. 5.3. On the extension of the hit-or-miss operator to grey tone images: two case studies depending on whether the origin of the composite SE belongs to B_{FG} or B_{BG}. In both diagrams, the centre of the pixels of each cross-section (or its complement) matched by the considered composite SE are marked with a bullet. When B_{FG} contains the origin, all these pixels belong to the subgraph of f while they all belong to the complement of the subgraph when the origin belongs to B_{BG}.

Fig. 5.3a at position $x = 8$, B_{FG} matches the cross-sections of f from the level 0 up to the level $t_{\mathrm{FG}} = 5$ while B_{BG} matches the complement of the cross-sections of f from the level $t_{\max}$ down to the level $t_{\mathrm{BG}} = 3$.

Depending on whether we constrain the SE component containing the origin to match either the foreground (if $\mathbf{o} \in B_{\mathrm{FG}}$) or the background (if $\mathbf{o} \in B_{\mathrm{BG}}$) of $\mathbf{x}$, we will obtain two different definitions for the grey tone

hit-or-miss transform. The first will be referred to as the *unconstrained* hit-or-miss. Accordingly, the previously mentioned constraint is at the basis of the *constrained* hit-or-miss. Fortunately, in the binary case, both definitions are equivalent and come down to Eq. 5.1.

Unconstrained hit-or-miss. The output of the *unconstrained hit-or-miss*, denoted by UHMT, of a grey scale image f by a composite SE $\mathbf{B}$ at a position $\mathbf{x}$ is defined as the number of cross-sections $\mathrm{CS}_t(f)$ such that B_{FG} at $\mathbf{x}$ matches $\mathrm{CS}_t(f)$ while, simultaneously, B_{BG} at $\mathbf{x}$ matches $\complement\mathrm{CS}_t(f)$:

$$\big[\mathrm{UHMT}_{\mathbf{B}}(f)\big](\mathbf{x}) = \mathrm{card}\{t \mid (B_{\mathrm{FG}})_{\mathbf{x}} \subseteq \mathrm{CS}_t(f),\ (B_{\mathrm{BG}})_{\mathbf{x}} \subseteq \complement\mathrm{CS}_t(f)\}. \quad (5.3)$$

Note that this latter equation comes down to cardinal number of the (possibly empty) intersection of the intervals $[0, t_{\mathrm{FG}}]$ and $[t_{\mathrm{BG}}, t_{\max}]$:

$$\begin{aligned}\big[\mathrm{UHMT}_{\mathbf{B}}(f)\big](\mathbf{x}) &= \mathrm{card}([0, t_{\mathrm{FG}}] \cap [t_{\mathrm{BG}}, t_{\max}]),\\ &= \begin{cases} t_{\mathrm{FG}} - t_{\mathrm{BG}} + 1, & \text{if } t_{\mathrm{FG}} \geq t_{\mathrm{BG}}.\\ 0, & \text{otherwise.}\end{cases}\end{aligned}$$

where $[t_i, t_j] \in \mathbb{N}_0$, $t_{\mathrm{FG}} = \max\{t \mid (B_{\mathrm{FG}})_{\mathbf{x}} \subseteq \mathrm{CS}_t(f)\}$, and $t_{\mathrm{BG}} = \min\{t \mid (B_{\mathrm{BG}})_{\mathbf{x}} \subseteq \complement\mathrm{CS}_t(f)\}$. In addition, $\max\{t \mid (B_{\mathrm{FG}})_{\mathbf{x}} \subseteq \mathrm{CS}_t(f)\}$ is nothing but the value of the erosion of f by B_{FG} at the position $\mathbf{x}$ while, similarly, $\min\{t \mid (B_{\mathrm{BG}})_{\mathbf{x}} \subseteq \complement\mathrm{CS}_t(f)\}$ equals 1 *plus* the value of the dilation of f by B_{BG} at the position $\mathbf{x}$. This leads to an equivalent formulation in terms of erosions and dilations and which is directly suitable for implementation purposes:

$$\begin{aligned}&\big[\mathrm{UHMT}_{\mathbf{B}}(f)\big](\mathbf{x}) = \\ &\begin{cases}\big[\varepsilon_{B_{\mathrm{FG}}}(f)\big](\mathbf{x}) - \big[\delta_{B_{\mathrm{BG}}}(f)\big](\mathbf{x}), & \text{if } \big[\delta_{B_{\mathrm{BG}}}(f)\big](\mathbf{x}) < \big[\varepsilon_{B_{\mathrm{FG}}}(f)\big](\mathbf{x}).\\ 0, & \text{otherwise.}\end{cases}\end{aligned} \quad (5.4)$$

Although the stacking of the hit-or-miss of the cross-sections of an image does not form the subgraph of a grey tone image, it can be observed that UHMT is in fact invariant to threshold decomposition: $\mathrm{UHMT}_{\mathbf{B}} = \sum_{t=1}^{t_{\max}} \mathrm{UHMT}_{\mathbf{B}}(\mathrm{CS}_t)$.

The unconstrained hit-or-miss transforms of the 1-D signal presented in Fig. 5.3 by the SEs $\mathbf{B}$ and $\mathbf{B}^c$ are displayed in Fig. 5.4. The unconstrained hit-or-miss transform is illustrated on a 2-D image in Fig. 5.5. The input image shows a honeycomb (hexagonal tessellation). We are interested in extracting all upper corner points of each hexagonal cell. This is achieved by performing the unconstrained hit-or-miss transform of the input image with the composite SE displayed in Fig. 5.5b. The threshold of the resulting image for all nonzero values highlights the performance of the detection.

Constrained hit-or-miss. The definition of the constrained hit-or-miss, denoted by CHMT, involves an additional constraint, considered for each pixel position $\mathbf{x}$. Namely, the SE component containing the origin $\mathbf{o}$ must

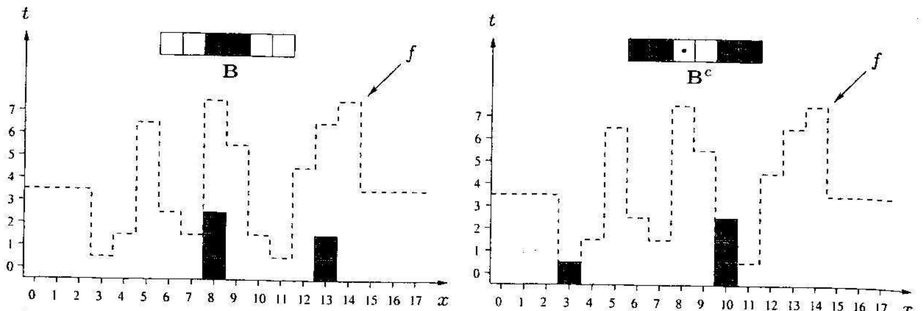

(a) $\mathrm{UHMT}_{\mathbf{B}}(f)$. (b) $\mathrm{UHMT}_{\mathbf{B}^c}(f)$.

Fig. 5.4. Grey scale unconstrained hit-or-miss transform of the 1-D signal f (see also Fig. 5.3). The graph of f appears as a dashed line.

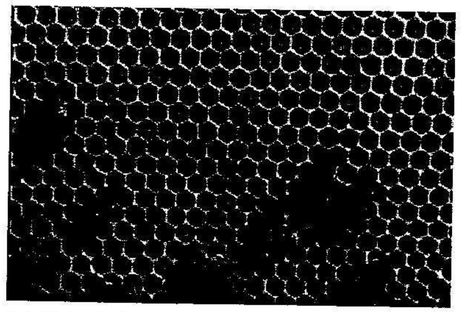

(a) 384×256 image f of a honeycomb illustrating the hexagonal tessellation.

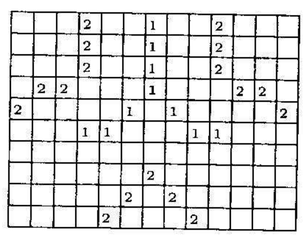

(b) Composite SE $\mathbf{B}$ with pixels of B_{FG} at 1 and B_{BG} at 2. The origin is the bold 1 pixel.

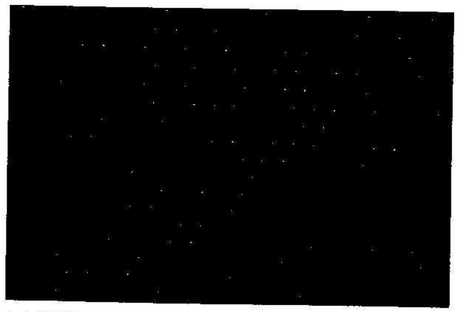

(c) $\mathrm{UHMT}_{\mathbf{B}}(f)$.

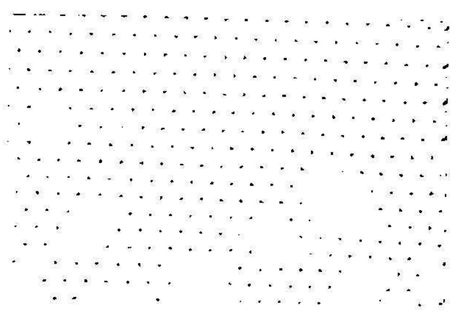

(d) Threshold of $\mathrm{UHMT}_{\mathbf{B}}(f)$ for all nonzero values: $T_{t>0}[\mathrm{UHMT}_{\mathbf{B}}(f)]$.

Fig. 5.5. Grey scale unconstrained hit-or-miss transform extracting the upper corner of each hexagonal cell appearing in the input image.

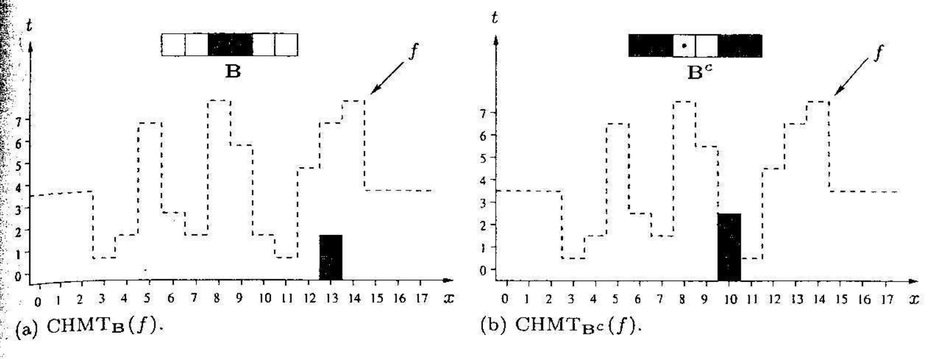

(a) $\mathrm{CHMT}_{\mathbf{B}}(f)$. (b) $\mathrm{CHMT}_{\mathbf{B}^c}(f)$.

Fig. 5.6. Grey scale constrained hit-or-miss transform of the 1-D signal f (see also Fig. 5.3). The graph of f appears as a dashed line.

match the foreground $\overline{\mathrm{FG}}(\mathbf{x})$ if $\mathbf{o} \in B_{\mathrm{FG}}$ or the background $\overline{\mathrm{BG}}(\mathbf{x})$ if $\mathbf{o} \in B_{\mathrm{BG}}$ (see page 34 for the definitions of $\overline{\mathrm{FG}}$ and $\overline{\mathrm{BG}}$). As for a graphical representation and looking back to Fig. 5.3, we only consider the t-connected components[1] of pixels marked by a bullet and which have a nonempty intersection with the t-boundary of the subgraph of f. This happens for $x = 13$ in Fig. 5.3a and $x = 10$ in Fig. 5.3b. In terms of morphological transformations, when $\mathbf{o} \in B_{\mathrm{FG}}$, $(B_{\mathrm{FG}})_{\mathbf{x}} \subseteq \overline{\mathrm{FG}}(\mathbf{x})$ if and only if $f(\mathbf{x}) = \big[\varepsilon_{B_{\mathrm{FG}}}(f)\big](\mathbf{x})$. Accordingly, when $\mathbf{o} \in B_{\mathrm{BG}}$, $(B_{\mathrm{BG}})_{\mathbf{x}} \subseteq \overline{\mathrm{BG}}(\mathbf{x})$ if and only if $f(\mathbf{x}) = \big[\delta_{B_{\mathrm{BG}}}(f)\big](\mathbf{x})$. By adding these constraints in the formulation of the unconstrained hit-or-miss (Eq. 5.4), we obtain the following definition for the constrained hit-or-miss CHMT:

$$\big[\mathrm{CHMT}_{\mathbf{B}}(f)\big](\mathbf{x}) = \qquad (5.5)$$
$$\begin{cases} f(\mathbf{x}) - \big[\delta_{B_{\mathrm{BG}}}(f)\big](\mathbf{x}), & \text{if } f(\mathbf{x}) = \big[\varepsilon_{B_{\mathrm{FG}}}(f)\big](\mathbf{x}) \\ & \text{and } \big[\delta_{B_{\mathrm{BG}}}(f)\big](\mathbf{x}) < f(\mathbf{x}). \\ \big[\varepsilon_{B_{\mathrm{BG}}}(f)\big](\mathbf{x}) - f(\mathbf{x}), & \text{if } f(\mathbf{x}) = \big[\delta_{B_{\mathrm{FG}}}(f)\big](\mathbf{x}) \\ & \text{and } \big[\varepsilon_{B_{\mathrm{BG}}}(f)\big](\mathbf{x}) > f(\mathbf{x}). \\ 0, & \text{otherwise.} \end{cases}$$

Note that, depending on whether the origin of $\mathbf{B}$ belongs to B_{FG} (resp. B_{BG}) only the first (resp. second) test must be considered. The constrained hit-or-miss transforms of the 1-D signal presented in Fig. 5.3 by the SEs $\mathbf{B}$ and $\mathbf{B}^c$ are displayed in Fig. 5.6.

Both definitions of the grey tone hit-or-miss are equivalent in the binary case and come down to Eq. 5.1. In the grey scale case, they are equivalent only in situations where the component of $\mathbf{B}$ containing the origin is restricted to a single pixel. The constrained hit-or-miss is by definition more restrictive than the unconstrained one as highlighted by the following ordering relationship:

[1] We call *t-connectivity* the 1-D dimensional connectivity defined along the discrete t-axis for a fixed value of x, i.e., $(\mathbf{x}_1, t_1)$ is t-connected to $(\mathbf{x}_2, t_2)$ if and only if $\mathbf{x}_1 = \mathbf{x}_2$ and $|t_1 - t_2| = 1$.

$\mathrm{CHMT}_{\mathbf{B}} \leq \mathrm{UHMT}_{\mathbf{B}}$. The hit-or-miss (whether unconstrained or constrained) by $\mathbf{B}$ is complementary to that by $\mathbf{B}^c$: $\mathrm{HMT}_{\mathbf{B}} = \mathrm{HMT}_{\mathbf{B}^c}$. Both types of HMT are non-increasing transformations.

In practice, the choice between the constrained or unconstrained hit-or-miss is application driven. In the sequel, we will keep using the notation HMT to refer to an arbitrary hit-or-miss, i.e., it can be substituted by either UHMT or CHMT in the grey scale case. Note that the substitution may be context dependent. For example, when dealing with the notion of homotopic thinning or thickening, the underlying hit-or-miss is always in the sense of a constrained hit-or-miss.

5.1.3 Applications

The hit-or-miss transformation is often used to detect specific configurations of pixels. Some interesting configurations are described hereafter. We then show that a series of hit-or-miss transforms with carefully selected composite SEs can be used to compute the connectivity number of an image.

Basic neighbourhood configurations.

- *Isolated foreground pixels* are defined as pixels having no foreground neighbours. The corresponding composite SE is a single pixel for B_{FG} with its neighbours for B_{BG}. It follows that the set B_{BG} will depend on the graph used for processing the image (see Fig. 5.1). The configuration is referred to by the letter **I** of Golay's alphabet (see table 5.2, page 158): $\mathbf{I} = (p, N_G(p))$, the origin being located at p. $\mathbf{I}^c$ is used for extracting isolated background pixels.
- *Foreground endpoints* are defined as foreground pixels having at most one object pixel among their neighbour pixels. They are usually used for extracting extremities of one-pixel thick curves. These pixels have the configuration **E** in the Golay's alphabet (see table 5.2, page 158). The extraction of the endpoints of a binary image is illustrated in Fig. 5.7.
- *Multiple foreground points* are defined as foreground pixels having more than two foreground pixels among their neighbour pixels. According to this definition of a multiple point, only foreground pixels are considered in the neighbouring configuration. Consequently, B_{BG} does not play a role and the hit-or-miss transform comes down to an erosion by B_{FG}. Multiple points are used for detecting connections between one-pixel width curves such as those obtained after a homotopic skeletonisation (see Sec. 5.5.2).
- *Foreground contour points* are foreground pixels having at least one background pixel among their neighbour pixels.

Connectivity number. Another interesting application of hit-or-miss transforms concerns the computation of the *connectivity number* of a binary image. This number refers to the number of connected components of the image minus the number of connected holes of these connected components. If there

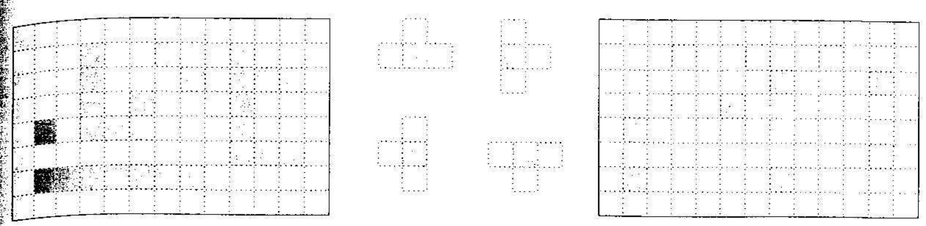

(a) Input image (b) SEs for 4-connected endpoints (c) Endpoints of input image

Fig. 5.7. Extraction of 4-connected foreground endpoints of a binary image (a). In the 4-connected square grid, there are four configurations (b) corresponding to an endpoint. (1 fundamental and its rotations of 45, 90, and 135 degrees). All endpoints (c) are obtained by performing hit-or-miss transforms in parallel with each SE and then unioning the results: $\bigcup_i \mathrm{HMT}_{\Theta_i \mathbf{B}}(X)$.

are no holes, the connectivity number of the image is equivalent to the number of image objects. Euler showed that the connectivity number of a surface is equal to the number of vertices v minus the number of edges e plus the number of faces f when the surface is divided into faces by means of vertices and edges in such a way that each face is topologically equivalent to a plane polygon:

$$\text{Connectivity Number} = v - e + f. \tag{5.6}$$

The connectivity number is also known as the Euler characteristic. Consider for instance a binary image in the hexagonal graph. Equation 5.6 tells us that the connectivity number of this image equals the number v_6 of object pixels of the image minus the number e_6 of edges of the hexagonal graph linking object pixels plus the number f_6 of elementary triangles of the graph having object pixels as vertices.

Let $\mathcal{N}()$ denote the number of pixels having the configuration specified within the parentheses. It is therefore obtained by counting the number of pixels remaining after the hit-or-miss transform with this configuration. We have therefore the following relationships:

$$\begin{aligned} v_6 &= \mathcal{N}(1), \\ e_6 &= \mathcal{N}\begin{pmatrix} 1 & 1 \end{pmatrix} + \mathcal{N}\begin{pmatrix} 1 \\ 1 \end{pmatrix} + \mathcal{N}\begin{pmatrix} 1 & \\ & 1 \end{pmatrix}, \\ f_6 &= \mathcal{N}\begin{pmatrix} 1 & 1 \\ 1 & 1 \end{pmatrix} + \mathcal{N}\begin{pmatrix} 1 & 1 \\ & 1 \end{pmatrix}. \end{aligned}$$

After expansion[2] and simplification, one finds:

$$v_6 - e_6 + f_6 = \mathcal{N}\begin{pmatrix} 0 & \\ 1 & 0 \end{pmatrix} - \mathcal{N}\begin{pmatrix} 1 & 0 \\ & 1 \end{pmatrix}.$$

[2] For example, $\mathcal{N}(1) = \mathcal{N}\begin{pmatrix} 1 & 1 \\ 1 & 1 \end{pmatrix} + \mathcal{N}\begin{pmatrix} 1 & 0 \\ 1 & 1 \end{pmatrix} + \mathcal{N}\begin{pmatrix} 1 & 1 \\ 1 & 0 \end{pmatrix} + \mathcal{N}\begin{pmatrix} 1 & 0 \\ 1 & 0 \end{pmatrix}$.

The formulæ for calculating the connectivity number in four different digital graphs are summarised in table 5.1. The connectivity number is therefore

Table 5.1. Connectivity number obtained by computing the number of pixels having specific configurations. $\mathcal{N}()$ denotes the number of pixels having the configuration specified within the parentheses.

Digital graph	Connectivity number
1-D	$\mathcal{N}($  $) - \mathcal{N}($  $)$
Hexagonal	$\mathcal{N}($ $) - \mathcal{N}($  $)$
4-connected	$\mathcal{N}($ $) + \mathcal{N}($  $) - \mathcal{N}($  $)$
8-connected	$\mathcal{N}($ $) - \mathcal{N}($  $)$

obtained by counting the number of pixels remaining after the hit-or-miss transform with the displayed configurations. Note that in 1-D, the concept of hole does not hold and therefore the connectivity number comes down to the number of connected components.

Using these formulæ to compute the connectivity number of Fig. 5.7a, it can be seen that it equals 5 for the 4-connected graph and 4 for the 8-connected graph. In this example, the connectivity number corresponds to the number of image objects because the image objects do not contain any hole. When there are holes, the number of connected components of the image can be obtained through a connected component labelling technique (see page 37). By subtracting the connectivity number from the number of connected components, we get the number of holes. Note that, as detailed in Sec. 2.6.2, 8-connectivity for foreground pixels and 4-connectivity for background pixels must be considered or vice versa.

The connectivity number of a connected set is an interesting shape descriptor that can be used together with other features for pattern recognition purposes. It applies directly to grey scale images but rather than counting the number of pixels of the hit-or-miss by the SEs given in table 5.1, the volume measurement (sum of grey levels) of the *unconstrained* hit-or-miss must be considered. For example, the 8-connectivity number of a grey scale image f is defined as follows:

$$\mathrm{V}[\mathrm{UHMT}_{\square}(f)] - \mathrm{V}[\mathrm{UHMT}_{\square}(f)]. \tag{5.7}$$

The resulting number comes down to the sum of the connectivity number of each cross-section of f. We will see in Chap. 11 that the connectivity number of a grey tone image may be used as a discriminant texture feature.

5.1.4 Hit-or-miss opening

In some applications it may be interesting to keep all points that fit the set rather than preserving the sole origin point when B_{FG} fits the foreground and, simultaneously, B_{BG} fits the background. This can be achieved by dilating the hit-or-miss transform by the reflection of B_{FG}. We call this transformation a *hit-or-miss opening* and denote it by $\tilde{\gamma}$:

$$\tilde{\gamma}_{\mathbf{B}} = \delta_{\check{B}_{\mathrm{FG}}} \mathrm{HMT}_{\mathbf{B}}. \tag{5.8}$$

As for openings, the hit-or-miss opening is independent of the position of the origin of the SE. It is also anti-extensive and idempotent but it is not an opening because it does not satisfy the required increasingness property.

The hit-or-miss opening is illustrated in Fig. 5.8. Figure 5.8a represents a binary image. A composite SE with a 2×2 square for the set of object pixels and its 4-connected neighbours for the set of background pixels is shown in Fig. 5.8b. All pixels of the binary image having the same configuration as the SE are given in Fig. 5.8c. In the grey scale case, depending on whether

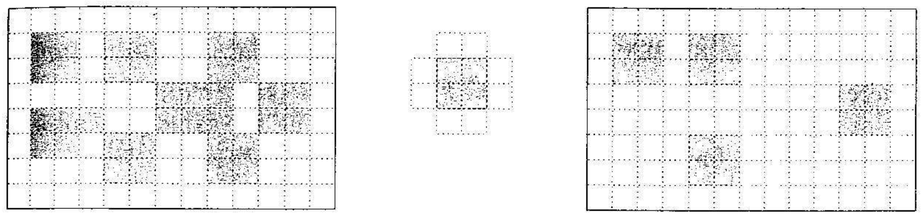

(a) Input image (b) A composite SE (c) Hit-or-miss opening of (a)

Fig. 5.8. Hit-or-miss opening of a binary image using a composite SE.

an unconstrained and constrained hit-or-miss is considered in Eq. 5.8, one obtains an unconstrained or constrained hit-or-miss opening. For example, the grey scale unconstrained hit-or-miss opening of the honeycomb shown in Fig. 5.5a using the composite SE described in Fig. 5.5b is displayed in Fig. 5.9 together with its threshold for all nonzero values.

By definition, the hit-or-miss opening is a subset of the morphological opening by B_{FG}: $\tilde{\gamma}_{\mathbf{B}} \leq \gamma_{B_{\mathrm{FG}}}$. A similar transformation can be defined by dilating the hit-or-miss transform by the reflection of B_{BG}. This operator corresponds to a hit-or-miss opening of the *background* of the image:

$$\tilde{\gamma}_{\mathbf{B}^c}(\mathsf{C}) = \delta_{\check{B}_{\mathrm{BG}}} \mathrm{HMT}_{\mathbf{B}}.$$

The dual transformation with respect to set complementation is called the hit-or-miss closing. It is denoted by $\tilde{\phi}$.

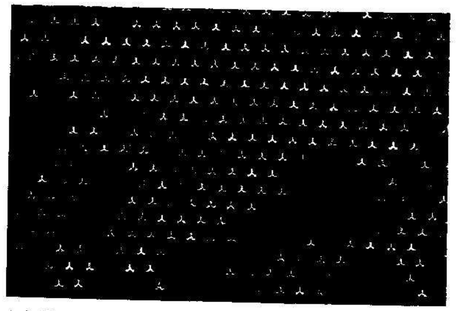

(a) Grey scale unconstrained hit-or-miss opening.

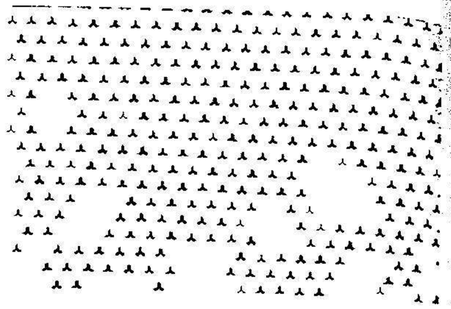

(b) Threshold of *(a)* for all nonzero values.

Fig. 5.9. Grey scale unconstrained hit-or-miss opening of the honeycomb image shown in Fig. 5.5a using the SE depicted in Fig. 5.5b.

5.1.5 Rank hit-or-miss

The hit-or-miss transform can be generalised by substituting the inclusion conditions in Eq. 5.1 with partial fit constraints. The resulting operation is called *rank hit-or-miss transform* with a composite SE $\mathbf{B}$ and the associated rank vector $\mathbf{k} = (k_{\mathrm{FG}}, k_{\mathrm{BG}})$:

$$\mathrm{HMT}_{\mathbf{B},\mathbf{k}}(X) = \zeta_{B_{\mathrm{FG}},k_{\mathrm{FG}}}(X) \cap \zeta_{B_{\mathrm{BG}},k_{\mathrm{BG}}}(X^c),$$

where $k_{\mathrm{FG}} \in \{1,\ldots,\mathrm{card}(B_{\mathrm{FG}})\}$ and $k_{\mathrm{BG}} \in \{1,\ldots,\mathrm{card}(B_{\mathrm{BG}})\}$. The rank hit-or-miss extends directly to grey scale images using the same principles as those described for the hit-or-miss:

$$\big[\mathrm{UHMT}_{\mathbf{B},\mathbf{k}}(f)\big](\mathbf{x}) = \begin{cases} \big[\zeta_{B_{\mathrm{FG}},k_{\mathrm{FG}}}(f)\big](\mathbf{x}) - \big[\zeta_{B_{\mathrm{BG}},k'_{\mathrm{BG}}}(f)\big](\mathbf{x}), \\ \qquad\qquad \text{if } \big[\zeta_{B_{\mathrm{BG}},k'_{\mathrm{BG}}}(f)\big](\mathbf{x}) < \big[\zeta_{B_{\mathrm{FG}},k_{\mathrm{FG}}}(f)\big](\mathbf{x}). \\ 0, \qquad\qquad \text{otherwise,} \end{cases} \tag{5.9}$$

where $k'_{\mathrm{BG}} = n_{\mathrm{BG}} - k_{\mathrm{BG}} + 1$ and $n_{\mathrm{BG}} = \mathrm{card}(B_{\mathrm{BG}})$. It follows that $\mathrm{HMT}_{\mathbf{B}} = \mathrm{HMT}_{\mathbf{B},(1,1)}$. Similarly, the *rank hit-or-miss opening* is defined as follows:

$$\tilde{\gamma}_{\mathbf{B},\mathbf{k}} = \mathsf{id} \wedge \delta_{\check{B}_{\mathrm{FG}}} \mathrm{HMT}_{\mathbf{B},\mathbf{k}}.$$

Rank-based hit-or-miss transforms are performing better than the corresponding plain hit-or-miss transforms in situations where the shape and size of the searched objects are approximatively known and possibly corrupted by external factors.

5.2 Thinning and thin-fit

Thinnings consist in removing foreground image pixels matching a configuration given by a composite SE. In other words, the hit-or-miss transform

of the image by this SE is subtracted from the original image. The thin-fit transform proceeds the same way but here it is a set of foreground pixels having a given configuration that is removed from the original image. That is, the hit-or-miss opening by the considered composite SE is subtracted from the input image. Formal definitions are presented hereafter. We then detail the notion of homotopic thinning.

5.2.1 Generic definitions

The *thinning* of an image f by a composite SE $\mathbf{B}$ is denoted[3] by $f \circ B$ or $\mathrm{THIN}_{\mathbf{B}}(f)$ and defined as the arithmetic difference between f and the hit-or-miss transform of f by $\mathbf{B}$:

$$f \circ \mathbf{B} = \mathrm{THIN}_{\mathbf{B}}(f) = f - \mathrm{HMT}_{\mathbf{B}}(f). \tag{5.10}$$

That is, $\mathrm{THIN}_{\mathbf{B}} = \mathsf{id} - \mathrm{HMT}_{\mathbf{B}}$. The origin of the SE must belong to the set B_{FG} of foreground pixels of $\mathbf{B}$, otherwise the thinning would come down to the identity transformation. Recall that HMT can be substituted by UHMT (resp. CHMT) so as to generate the definition of the unconstrained thinning UTHIN (resp. constrained thinning CTHIN). For example, starting from the definition of the constrained hit-or-miss (Eq. 5.14), we obtain the following formulation for the constrained thinning:

$$\big[\mathrm{CTHIN}_{\mathbf{B}}(f)\big](\mathbf{x}) = \begin{cases} \big[\delta_{B_{\mathrm{BG}}}(f)\big](\mathbf{x}), \text{ if } \big[\delta_{B_{\mathrm{BG}}}(f)\big](\mathbf{x}) < f(\mathbf{x}) \text{ and } f(\mathbf{x}) = \big[\varepsilon_{B_{\mathrm{FG}}}(f)\big](\mathbf{x}), \\ f(\mathbf{x}), \qquad \text{otherwise.} \end{cases} \tag{5.11}$$

By construction, thinnings are anti-extensive and non-increasing operators. An example of grey scale thinning consists in performing a thinning with the SE designed for removing isolated pixels (see Fig. 5.1). This is achieved by thinning the grey scale image by the SE corresponding to isolated points. By doing so, each isolated image maximum (i.e., pixels whose neighbours have a strictly lower value) will be set to the largest value of their neighbours (see also Fig. 5.12).

The *thin-fit* of an image consists in computing the arithmetic difference between this image and its hit-or-miss opening with a composite SE. We denote this transformation by $\tilde{\bigcirc}$:

$$f \,\tilde{\bigcirc}\, \mathbf{B} = f - \tilde{\gamma}_{\mathbf{B}}(X).$$

We also use the functional notation $\widetilde{\mathrm{THIN}}$: $\widetilde{\mathrm{THIN}}_{\mathbf{B}} = \mathsf{id} - \tilde{\gamma}_{\mathbf{B}}$.

[3] Beware that in the literature, the symbol $\circ$ is sometimes used for the morphological opening operator (and $\bullet$ for the morphological closing).

5.2.2 Homotopic thinning

Some applications require procedures for thinning a pattern while preserving its homotopy. This idea is at the very basis of the notion of skeletonisation introduced in Sec. 5.4. In this section, we concentrate on the preliminary concept of homotopic thinning. Its use for generating discrete skeletons will be detailed in Secs. 5.5.2 and 5.5.3.

Simple pixel. A thinning by a given composite SE is said to be homotopic if it does not alter the homotopy of the input image. There is therefore a need for characterising the corresponding class of homotopic composite SEs. As the homotopy property relies on the notion of connectivity, we can restrict our analysis, without loss of generality, to SEs defined over the elementary neighbourhood of a pixel. We should also keep in mind that, for the square grid, if 8-connectivity is used for the foreground, 4-connectivity must be used for the background and vice versa (i.e., 8-neighbourhoods must be considered in any case for the square grid). In the following, $\mathcal{G}$ refers to the connectivity of the foreground pixels and $\mathcal{G}'$ to that of the background. That is, $\mathcal{G} = \mathcal{G}' = 6$ for the hexagonal graph while $\mathcal{G} = 4$ and $\mathcal{G}' = 8$ or vice versa for the square grid. Moreover, we denote by $\mathcal{G}_{\max}$ the maximum between $\mathcal{G}$ and $\mathcal{G}'$.

By definition, each homotopic composite SE $\mathbf{B}$ is such that B_{FG} contains the origin plus at least one neighbour pixel while all pixels of B_{BG} belong to the neighbourhood of the origin. The complete characterisation of a homotopic configuration can be answered by the notion of a simple (also called deletable) pixel.

A pixel p of a grey tone image f is $\mathcal{G}$-*simple* if and only if its set of background $\mathcal{G}'$-neighbours is nonempty and if, in addition, the image obtained by decreasing the value of this pixel from its original value $f(p)$ to the maximum value of its background $\mathcal{G}'$-neighbours $\max\{f(p') \mid p' \in N^{\leq}_{\mathcal{G}'}(p)\}$ is homotopic to the original image. We call *simpleness property* the property of being simple. Depending on whether a pixel is simple or not, the *simpleness test* returns true or false. An implementation of the simpleness test is as follows: a pixel p of an image f is $\mathcal{G}$-simple if and only if the two following conditions hold (see page 34 for the definitions of $N^{\geq}_{\mathcal{G}}$ and $N^{\leq}_{\mathcal{G}}$):

1. the set of foreground $\mathcal{G}_{\max}$-neighbours of p, $N^{\geq}_{\mathcal{G}_{\max}}(p)$, is nonempty and $\mathcal{G}$-connected;
2. the set of background $\mathcal{G}'$-neighbours of p, $N^{\leq}_{\mathcal{G}'}(p)$, is nonempty.

The class of $\mathcal{G}$-homotopic structuring elements is therefore defined as the set of all neighbourhood configurations whose $\mathcal{G}$-simpleness test returns true. Figure 5.10 displays the 256 neighbourhood configurations of a foreground pixel while highlighting those that are homotopic in the practical framework whereby 8-connectivity is used for the foreground and therefore 4-connectivity for the background (i.e., $\mathcal{G} = 8$ and $\mathcal{G}' = 4$). In other words, the 8-simpleness test returns true for all image pixels matching a configuration highlighted by a dark grey frame in Fig. 5.10. In practice, a homotopic thinning is performed by computing a *constrained* thinning with a homotopic configuration. Indeed, an unconstrained thinning with a homotopic SE clearly leads to a non-homotopic transformation because the value of a pixel may be decreased irrespectively of its ordering relation with its foreground neighbours (with a constrained thinning, the pixel value must match the output of the erosion of the image with B_{FG} at this pixel). Therefore, when we refer to a 'homotopic thinning' it is always in the sense of a constrained thinning.

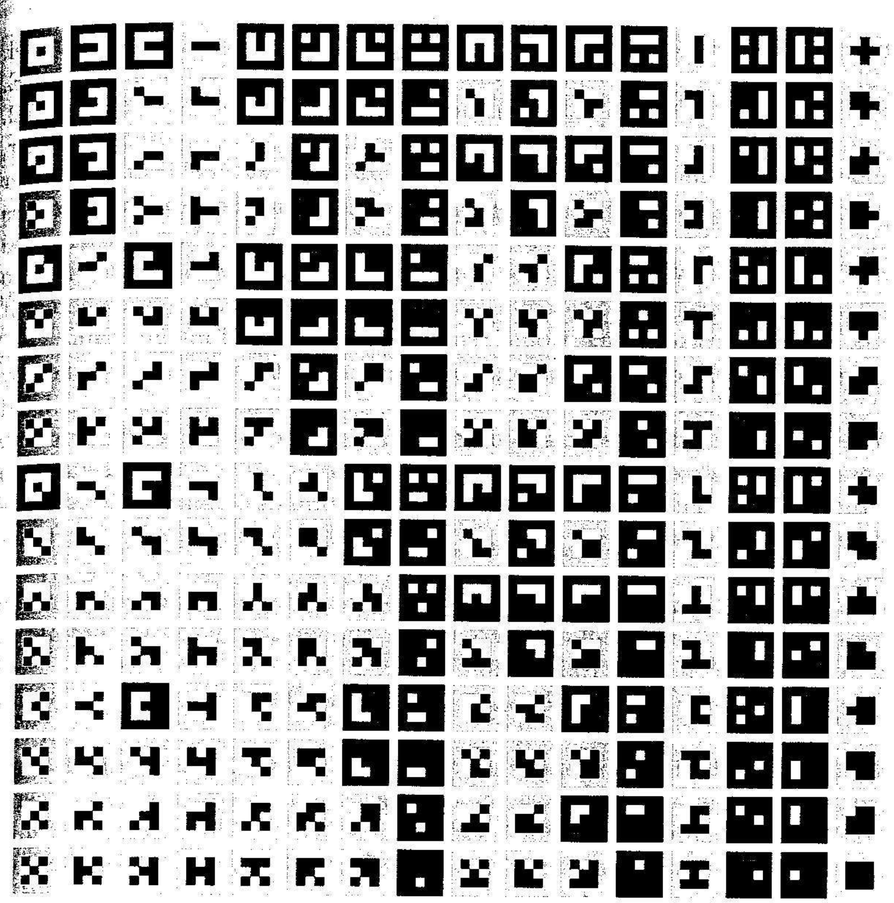

Fig. 5.10. The 256 possible 8-neighbourhood configurations of a foreground pixel of the square grid. Pixels of B_{FG} appear in black, while pixels of B_{BG} are displayed in white. The homotopic configurations in the case of 8-connectivity for the foreground and therefore 4-connectivity for the background are those highlighted by a dark grey frame.

Order independent simple pixel. In practice, simple pixels of an image cannot be retrieved in parallel because this may change the homotopy of the input image. For example, all pixels of a 2 pixel thick horizontal line are

simple and would therefore vanish if all simple pixels were deleted in parallel. A first solution is to delete only those pixels matching a given homotopic SE. This idea is at the basis of the sequential thinnings introduced in Sec. 5.5.2. Another approach consists in deleting the simple pixels in sequential order, one at a time, while taking into account this deletion when checking whether the subsequent pixels are simple or not. By definition, the resulting image is homotopic to the input image but it strongly depends on the sequence used for scanning the image pixels. For example, a rectangle would be reduced to its lower right pixel in the case of a sequential forward image scan whereas it is its upper left pixel which would remain for a backward image scan.

An order independent homotopic thinning algorithm can be obtained by deleting only those simple pixels of the original image which are deleted *whatever* the considered scanning order (i.e., for all possible scanning orders). These pixels are called *order independent simple pixels* and they are said to be *independent*. The notion of independence requires a careful analysis of adjacent simple pixels. Indeed, a simple pixel which does not contain any other simple pixel in its neighbourhood is clearly removed by all scanning orders. We now restrict our attention to the binary case, using 8-connectivity for the foreground and therefore 4-connectivity for the background and summarise the results developed in (Ranwez and Soille, 2002).

Let p and q be two simple 8-adjacent pixels. Then, p is said to be *independent* of q if and only if there is another foreground pixel within the intersection of their 8-neighbourhoods and, in addition, when p and q are 4-adjacent, p has a 4^0-neighbour 4-adjacent to a 4^0-neighbour of q. Therefore, if these conditions are not satisfied, p is said to be dependent of q in the sense that its deletion depends on whether q is removed beforehand or not. However, the fact that p is independent of q is not a sufficient condition for asserting that it will be removed by all scanning orders. This happens however if p is *strictly independent* of q. A simple pixel p is *strictly* independent of an 8-adjacent simple pixel q if and only if p is independent of q and, in addition, there is a *nonsimple* foreground pixel within the intersection of their 8-neighbourhoods. We still need to define what happens if an independent simple pixel p is independent of all its simple neighbours while being not strictly independent of at least one of them, denoted by q_1. It can be shown that, if p and q_1 are not in one of the four configurations (plus their rotations through $\pi/2$ and their symmetries with respect to the p–q_1 axis) displayed in Fig. 5.11, then there exists a scanning order where p is not removed. Otherwise, if $\mathrm{CC}_8^1(p)$ only contains simple pixels and if, in addition, it is strongly *8-deletable*[4], then there exists an order where p is not

[4] The 8-connected component of a foreground pixel p of a binary image X is denoted by $\overline{\mathrm{CC}}_8^1(p)$, Similarly, $\mathrm{CC}_8^1(p) = \overline{\mathrm{CC}}_8^1(p) \backslash p$. A given $\mathrm{CC}_8^1(p)$ is *strongly 8-deletable* if and only if it only contains simple pixels and, in addition, there exists a sequential scanning order of its pixels such that they can all be removed without modifying the homotopy, i.e., we can label the pixels of $\mathrm{CC}_8^1(p)$ as $q_1, \ldots, q_n$ in such a way that each q_i is simple in $X \setminus \{q_j \mid j < i\}$, where $n = \mathrm{card}[\mathrm{CC}_8^1(p)]$.

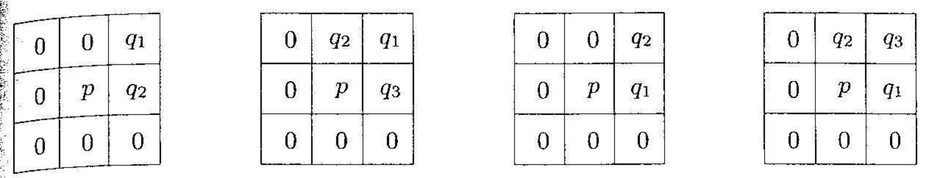

Fig. 5.11. Assuming that a pixel p is independent of all its simple neighbours q_i but is not strictly independent of at least one of them denoted by q_1, then if p does not match one of the displayed configurations (plus their rotations through $\pi/2$ and their symmetries with respect to the p–q_1 axis), there exists a scanning order where p will not be deleted. That is, the displayed configurations are a necessary but not sufficient condition to have p deleted for all scanning orders.

removed. If one of these latter two conditions is not satisfied, p is removed by all scanning orders. The full characterisation of simple pixels p can therefore be summarised as follows:

```
if p is dependent of one of its simple neighbours,
    then there exists a scanning order where p will not be removed.
else if p is strictly independent of all its simple neighbours,
    then p will be removed by all scanning orders.
else if p and q1 are not in one of the configurations of Fig. 5.11,
    then there exists an order where p is not removed.
else if CC8^1(p) only contains simple pixels and is strongly 8-deletable,
    then there exists an order where p is not removed.
else p will be removed by all scanning orders.
```

All these developments are at the basis of the notion of order independent skeleton detailed in Sec. 5.5.3.

5.3 Thickening and thick-miss

A thickening consists in adding background pixels having a specific configuration to the set of foreground pixels. This is achieved by adding to the input image the hit-or-miss transform by the corresponding composite SE. Similarly, the thick-miss is defined as the addition of the hit-or-miss opening of the background by the considered composite SE to the input image.

5.3.1 Generic definitions

The *thickening* of an image f by a composite SE $\mathbf{B}$ is denoted by $f \odot B$ or $\mathrm{THICK}_{\mathbf{B}}(f)$ and defined as the addition of f and the hit-or-miss transform of f by $\mathbf{B}$:

$$f \odot \mathbf{B} = \mathrm{THICK}_{\mathbf{B}}(f) = f + \mathrm{HMT}_{\mathbf{B}}(f). \tag{5.12}$$

That is, $\mathrm{THICK}_{\mathbf{B}} = \mathsf{id} + \mathrm{HMT}_{\mathbf{B}}$. The origin of the SE must belong to the set B_{BG} of background pixels of $\mathbf{B}$, otherwise the thickening would come down to

the identity transformation. Recall that HMT can be substituted by UHMT (resp. CHMT) so as to define the unconstrained thickening UTHICK (resp. constrained thickening CTHICK). For example, the constrained hit-or-miss (Eq. 5.14) leads to the following formulation:

$$\big[\mathrm{CTHICK}_{\mathbf{B}}(f)\big](\mathbf{x}) = \begin{cases} \big[\varepsilon_{B_{\mathrm{BG}}}(f)\big](\mathbf{x}), \text{ if } \big[\delta_{B_{\mathrm{FG}}}(f)\big](\mathbf{x}) = f(\mathbf{x}) \text{ and } f(\mathbf{x}) < \big[\varepsilon_{B_{\mathrm{BG}}}(f)\big](\mathbf{x}), \\ f(\mathbf{x}), \qquad \text{otherwise.} \end{cases}$$

By construction, thinnings are extensive and non-increasing operators. The dual transformation of the thinning by a composite SE $\mathbf{B}$ is the thickening by $\mathbf{B}^c$:

$$\mathrm{THIN}_{\mathbf{B}} = \complement \mathrm{THICK}_{\mathbf{B}^c} \complement. \tag{5.13}$$

The *thick-miss* transform is obtained by adding to the image the hit-or-miss opening of the background of this image. We denote this transformation by $\tilde{\odot}$:

$$f \,\tilde{\odot}\, \mathbf{B} = f + \tilde{\gamma}_{\mathbf{B}^c}(f^c).$$

We also use the functional notation $\widetilde{\mathrm{THICK}}$: $\widetilde{\mathrm{THICK}}_{\mathbf{B}} = \mathsf{id} + \tilde{\gamma}_{\mathbf{B}^c} \complement$.

Owing to the extensivity of the thickenings and the anti-extensivity of the thinnings, we can order thick-misses, thickenings, thinnings, and thin-fits with respect to the identity transformation as follows:

$$\widetilde{\mathrm{THIN}}_{\mathbf{B}} \leq \mathrm{THIN}_{\mathbf{B}} \leq \mathsf{id} \leq \mathrm{THICK}_{\mathbf{B}^c} \leq \widetilde{\mathrm{THICK}}_{\mathbf{B}^c}.$$

Note that, by construction, the following relationship holds:

$$\mathrm{HMT}_{\mathbf{B}} = \begin{cases} \mathsf{id} - \mathrm{THIN}_{\mathbf{B}}, & \text{if } \mathbf{o} \in B_{\mathrm{FG}}. \\ \mathrm{THICK}_{\mathbf{B}} - \mathsf{id}, & \text{otherwise.} \end{cases} \tag{5.14}$$

Finally, rank thinnings and thickenings are defined by using a 2-D vector $\mathbf{k}$ of ranks and adapting the corresponding definitions. For example, the output of the constrained rank thickening $\mathrm{CTHICK}_{\mathbf{B},\mathbf{k}}$ at the given pixel $\mathbf{x}$ is defined as follows:

$$\big[\mathrm{CTHICK}_{\mathbf{B},\mathbf{k}}(f)\big](\mathbf{x}) = \begin{cases} \big[\zeta_{B_{\mathrm{BG}},k_{\mathrm{BG}}}(f)\big](\mathbf{x}), & \text{if } \big[\delta_{B_{\mathrm{FG}},k_{\mathrm{FG}}}(f)\big](\mathbf{x}) = f(\mathbf{x}) \\ & \quad \text{and } f(\mathbf{x}) < \big[\varepsilon_{B_{\mathrm{BG}},k_{\mathrm{BG}}}(f)\big](\mathbf{x}), \\ f(\mathbf{x}), & \text{otherwise.} \end{cases}$$

The dual transformation defines the rank thinning operator. A practical implementation of the rank hit-or-miss follows directly:

$$\mathrm{HMT}_{\mathbf{B},\mathbf{k}} = \begin{cases} \mathsf{id} - \mathrm{THIN}_{\mathbf{B},\mathbf{k}}, & \text{if } \mathbf{o} \in B_{\mathrm{FG}}. \\ \mathrm{THICK}_{\mathbf{B},\mathbf{k}} - \mathsf{id}, & \text{otherwise.} \end{cases} \tag{5.15}$$

5.3.2 Examples

Interesting self-dual filters can be constructed using thickenings and thinnings with a pair of dual SEs. Consider for instance a thinning of the image with the SE $\mathbf{I}$ used removing isolated foreground pixels (see table 5.2) followed by a thickening with $\mathbf{I}^c$:

$$(f \circ \mathbf{I}) \odot \mathbf{I}^c.$$

The order of the sequence leads to identical results:

$$(f \circ \mathbf{I}) \odot \mathbf{I}^c = (f \odot \mathbf{I}^c) \circ \mathbf{I}.$$

Moreover, this transformation is self-dual, idempotent, and increasing. It is illustrated in Fig. 5.12 for the filtering impulse or salt-and-pepper noise. This

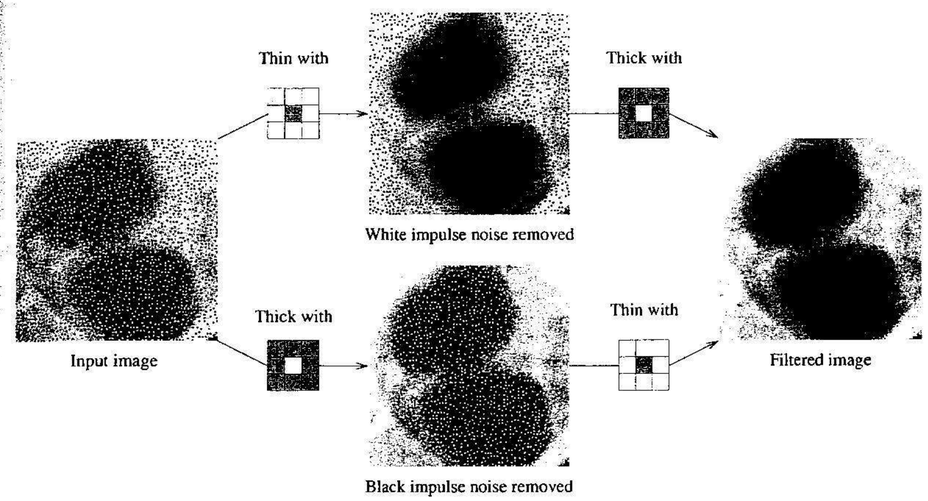

Fig. 5.12. Filtering of salt-and-pepper noise using a pair of grey scale thinning and thickening with the SE $\mathbf{I}$ of Golay's alphabet. This filter is idempotent, increasing, and self-dual. Note that the order of the thinning and thickening does not play a role.

filter is equivalent to a 8-connected surface area opening followed by a 8-connected surface area closing (or vice versa). Remember that median filters are also very efficient for filtering salt-and-pepper noise.

Another example is the computation of convex hulls in the sense of the strong convexity introduced in Sec. 2.6.5. The strong convex hull of an image f in the grid $\mathcal{G}$ is obtained by performing thickenings until stability with the composite SE $\mathbf{C}$ (and its rotations) of Golay's alphabet, see table 5.2. A thickening with a SE and its rotations is called a sequential thickening. It is denoted by $\underline{\odot}$. We have therefore the following relationship:

$$\mathrm{CH}_{\mathcal{G}}(f) = (f \,\underline{\odot}\, \mathbf{C})^{(\infty)},$$

Table 5.2. Various structuring elements used in the hexagonal graph for thinnings, thickenings, and hit-or-miss transformations. Grey hexagons represent object pixels and white hexagons background pixels. Complemented SEs must to be considered for the thickenings. The whole set of SEs corresponding to a given letter are obtained by considering the rotations of the displayed SE. The undisplayed neighbours of the origin of the displayed SEs are *don't care* pixels in the sense that they can match either the foreground or the background.

Neighbourhood configuration **B** (Golay alphabet)	Thinning (using **B**)	Thickening (using $\mathbf{B}^c$)	Hit-or-Miss
L [a]	Homotopic white skeleton.	Homotopic black skeleton.	–
M	Homotopic white skeleton starting from a hole.	Homotopic black skeleton starting from a point.	–
C	–	Strong convex hull.	–
D	Homotopic marking.	Homotopic nearly convex hull.	–
E [b]	Pruning of white skeletons.	Pruning of black skeletons.	Endpoints of skeletons.
I [c]	Remove isolated pixels.	Fill 1-pixel holes.	Isolated pixels.

[a] and for 4-connected, and for 8-connected skeletons.
[b] for 4-connected, and for 8-connected pruning.
[c] for 4-connected, for 8-connected isolated points.

where $f \underline{\odot} \mathbf{C} = (\cdots((f \odot \Theta_1\mathbf{C}) \odot \Theta_2\mathbf{C}) \odot \cdots) \odot \Theta_n\mathbf{C}$ and $\Theta_1, \Theta_2, \ldots, \Theta_n$ are the n possible discrete rotations of the SE **C**.

5.4 Euclidean skeletons

In pattern recognition and shape analysis, methods for extracting object features are needed. A classical approach consists in working on a contour representation of the object (Freeman, 1974). Another possibility is to thin the object to a set of lines condensing the information of the original object while preserving its homotopy. The resulting thin lines are called the *skeleton* or *medial axis* of the input pattern. The corresponding transformations are called *skeletonisation* or *medial axis transformation*. The detection of endpoints, multiple points, and closed loops of a skeleton is important for many shape recognition techniques such as those used for optical character recognition. Another typical use of skeletonisation algorithms occurs when

processing scanned documents containing line drawings such as those appearing in cadastral and topographical maps. Indeed, one needs to set the resolution according to the thickness of the printed lines so as to make sure that the scanned lines remain connected. Consequently, the scanned lines have a thickness greater than 1 pixel. Usually, scanned line drawings are vectorised because their representation in terms of a succession of arcs is much more efficient than a raster representation. However, vectorisation procedures require 1 pixel thick lines to correctly vectorise a line as a succession of arcs. This problem can be solved by reducing the thick lines to 1 pixel thick lines beforehand, i.e., by skeletonising the scanned line drawings.

Several formal definitions for the skeleton of a Euclidean set are available. Fortunately and contrary to what happens for discrete sets (see Sec. 5.5), they all lead to similar thin lines. Five different processes leading to the skeleton of a Euclidean set are briefly described hereafter.

5.4.1 Grass-fire or wavefront propagation

Assuming a fire or wavefront is starting from the contour points of a set X and propagating at uniform speed within the set, the *medial axis* or *skeleton* of X is the set of points where the fire or wavefronts meet. For example, the skeleton of a disc is its centre because all wavefronts meet simultaneously at its centre. The skeleton of a square corresponds to its diagonals, etc.

5.4.2 Distance function

The successive fronts of the fire propagation are equivalent to the successive distance levels of the distance transform on the set. The intensity surface of a distance transform has a maximal directional slope of one everywhere except along its ridges where it is undefined. The ridges of the distance function are equivalent to the set of points where the fire fronts meet (see definition in terms of grass-fire). These ridges are therefore equivalent to the skeleton.

The locus of the skeletal points together with their minimal distance to the boundary of the set is sometimes called the *quench function*.

5.4.3 Maximal discs

A disc B is maximal in X if there exists no other disc included in X and containing B. A necessary and sufficient condition for B to be maximal in X is that B is tangent to at least two distinct points of the boundary of X. The skeleton $\mathrm{SK}(X)$ of a set X is then defined by the centres of the maximal discs of X:

$$\mathbf{x} \in \mathrm{SK}(X) \Leftrightarrow$$
$$\exists \mathbf{y}_1, \mathbf{y}_2 \in \partial X \mid \mathbf{y}_1 \neq \mathbf{y}_2 \text{ and } d_\mathcal{E}(\mathbf{x}, \partial X) = d_\mathcal{E}(\mathbf{x}, \mathbf{y}_1) = d_\mathcal{E}(\mathbf{x}, \mathbf{y}_2),$$

where ∂X denotes the boundary of X.

5.4.4 Minimal paths

A minimal paths linking a point $\mathbf{x}$ of a set X to the boundary ∂X of this set is defined as a path having p and a point ∂X as endpoints and whose length equals the distance from $\mathbf{x}$ to ∂X. The skeleton of X corresponds to the points of X which do not belong to any other minimal path than those linking themselves to the boundary of X.

5.4.5 Openings

Lantuéjoul's formula (1978) states that the centres of the maximal discs of a set can be defined in terms of set differences between an erosion and its opening by discs B:

$$\mathrm{SK}(X) = \bigcup_{\lambda \geq 0} \bigcap_{\mu > 0} \Big\{ \varepsilon_{\lambda B}(X) \setminus \gamma_{\mu B}[\varepsilon_{\lambda B}(X)] \Big\}. \tag{5.16}$$

All these processes output almost identical skeletons and preserve the homotopy of the original set (provided that it is opened in the topological sense). Figure 5.13 illustrates the three first processes for the skeletonisation of a square.

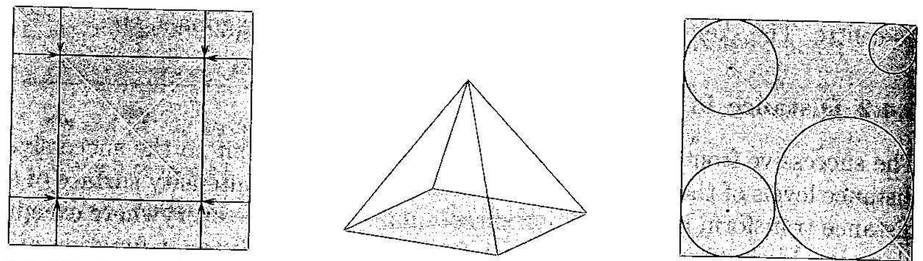

(a) Meeting points of wavefronts.

(b) Crest lines of the distance function.

(c) Centres of maximal discs.

Fig. 5.13. Skeletons of a continuous square using three different although equivalent approaches (the skeleton of a square corresponds to its diagonals).

The skeletonisation of a set is very sensitive to small variations of its boundary. For instance, a single notch along the boundary of a rectangle creates two new skeleton branches. It follows that a set must be filtered before computing its skeleton. Post-filtering can also be considered to remove irrelevant branches of a skeleton.

The skeleton of a n-gon contains n branches. By increasing the number of sides of a regular n-gon, it will tend to a disc but its skeleton does not tend to the skeleton of a disc since the number of branches increases with n. These two examples illustrate that the skeletonisation is not a continuous image transform: $X \to Y \not\Rightarrow \mathrm{SK}(X) \to \mathrm{SK}(Y)$. It is however an anti-extensive and idempotent image transformation (but non-increasing).

5.5 Discrete skeletons

The extension of the notion of skeleton to discrete sets is not straightforward. Indeed, notions such as wave propagations or discs have no direct and unique discrete equivalent. Moreover, on one hand a discrete skeletal line is not infinitely thin since it has a thickness of at least one pixel and on the other hand one pixel thin and centred skeleton are two mutually incompatible properties (consider for example the skeleton of a 2 pixel thick discrete line). It follows that adaptations of the definitions presented in the continuous space lead to a wide variety of skeletons which do not share the same properties. Five different discrete skeleton definitions are detailed in this section. Two practical applications are then described.

5.5.1 Openings

Consider for instance the skeletonisation in terms of openings by adapting Eq. 5.16 to the digital framework using the elementary symmetric SE B as a digital approximation of a disc of size 1:

$$\mathrm{SK}(X) = \bigcup_{\lambda \geq 1} \Big\{ \varepsilon_{\lambda B}(X) \setminus \gamma_B[\varepsilon_{\lambda B}(X)] \Big\} = \bigcup_{\lambda \geq 1} \Big\{ \mathrm{WTH}_B[\varepsilon_{\lambda B}(X)] \Big\}. \tag{5.17}$$

For example, B is the elementary square of width 3 and λB is a square of width $2\lambda + 1$ (see Eq. 3.7). Note that Eq. 5.17 corresponds to the union of the white top-hats of the successive erosions of the original set. By definition, there is a one-to-one correspondence between the skeleton by opening and the centres of the maximal λB in X. In addition, because B is defined by the elementary symmetric SE of the considered grid (i.e., it matches the neighbourhood $\overline{N}_{\mathcal{G}}$), it can be shown that, in the binary case, the skeleton by opening is equivalent to the centres of the $\mathcal{G}$-connected local maxima[5] of the discrete distance function $D_{\mathcal{G}}$:

$$\mathrm{SK}(X) = \big\{ p \in X \mid \forall p' \in N_{\mathcal{G}}(p),\ [D_{\mathcal{G}}(X)](p') \leq [D_{\mathcal{G}}(X)](p) \big\}. \tag{5.18}$$

The skeleton by opening using squares (i.e., $B = \overline{N}_8$) is illustrated in Fig. 5.14. Each pixel of the skeleton is also the centre of a maximal symmetric square and a local maximum of D_8. The resulting skeleton is not connected and the width of its branches equals one or two pixels depending on whether the width of the original structure is odd or even. This is not a problem for coding issues. Indeed, by storing the size at which each skeletal pixel appears, one can reconstruct the original shape. More precisely, denoting by $\mathbf{s}$ a point of the discrete skeleton by opening of a set X, $\lambda_{\mathbf{s}}$ the size at which it appeared,

[5] A pixel p of an image f is defined as a *$\mathcal{G}$-connected local maximum* if and only if none of its $\mathcal{G}$-neighbours have a greater grey scale value: $\forall p' \in N_{\mathcal{G}}(p),\ f(p') \leq f(p)$.

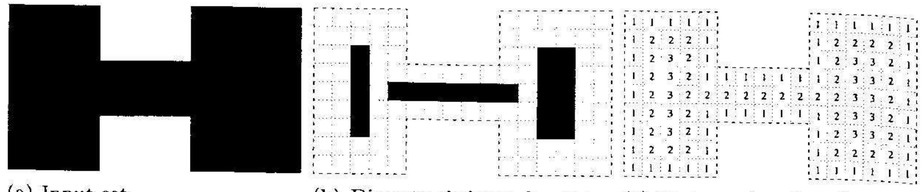

(a) Input set (b) Discrete skeleton by opening with squares (c) Distance function D_8

Fig. 5.14. Discrete skeleton by opening of an original set using discrete squares of increasing size according to Eq. 5.17. Note that the skeleton is *not* homotopic to the original set nor of width of 1 pixel. The opening size λ at which the horizontal branch appears equals 1. It equals 2 for both vertical branches. These branches are also matched by the local maxima of the distance function D_8.

and $(\lambda_{\mathbf{s}}B)_{\mathbf{s}}$ the structuring element B of size $\lambda_{\mathbf{s}}$ centred at $\mathbf{s}$, we obtain the following reconstruction formula:

$$X = \bigcup_{\mathbf{s}\in \mathrm{SK}(X)} (\lambda_{\mathbf{s}}B)_{\mathbf{s}}.$$

Note that the definition of the skeleton by opening as per Eq. 5.17 is directly suited to the processing of grey tome images.

5.5.2 Homotopic sequential thinnings

A non-connected skeleton is useless for shape description applications since the homotopy is not preserved and characteristic points such as multiple points and endpoints encountered in the continuous case are lost. A digital set can be skeletonised so as to preserve these important properties by thinning the set with SEs preserving the homotopy, i.e., homotopic SEs. The approach described in this section is referred to as skeletonisation by *sequential* homotopic thinning because the image is iteratively thinned by a sequence of homotopic SEs (and their rotations) until stability is reached. A *sequential thinning* of a binary image X by a composite SE $\mathbf{B}$ and its n possible discrete rotations is denoted by $X \underline{\circ} \mathbf{B}$:

$$X \underline{\circ} \mathbf{B} = (\cdots((X \circ \Theta_1\mathbf{B}) \circ \Theta_2\mathbf{B}) \circ \cdots) \circ \Theta_n\mathbf{B}.$$

The homotopic SEs $\mathbf{D}$, $\mathbf{L}$, and $\mathbf{M}$ (and their rotations by $n60^o$, where $n = 1,\ldots,5$) of Golay's alphabet displayed in table 5.2 match all 30 possible homotopic SEs of the hexagonal graph. A different type of skeleton is defined for each homotopic SE. For example, the $\mathbf{L}$-skeleton is obtained by thinning the input image with the six rotations of $\mathbf{L}$ until idempotence:

$$\mathrm{SK}_{\mathbf{L}}(X) = (X \underline{\circ} \mathbf{L})^{(\infty)}. \tag{5.19}$$

An example of binary $\mathbf{L}$-skeleton is provided in Fig. 5.15a. The output skeleton not only depends on the chosen homotopic SE but also on the rotation order defined in the sequential thinning. In the square grid, the skeletonisation of 4-connected objects is obtained by thinning the image with the following two SEs and their four rotations:  and  . 8-connected skeletons are obtained with the following SEs:  and  . The computation of skeletons using thinnings is directly suited to the processing of grey scale images. For example, the 4-connected grey tone skeleton displayed in Fig. 5.15b has been computed using the following sequence: $[(f \underline{\circ}$ $) \underline{\circ}$ $]^{(\infty)}$.

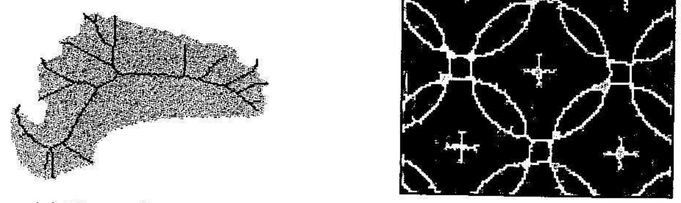

(a) Binary L-skeleton (b) Grey scale skeleton of Fig. 4.9a

Fig. 5.15. Binary and grey tone skeletons using sequential homotopic thinnings until stability.

In some applications, it is useful to reduce an image to the smallest possible image while preserving the homotopy of the input image. This procedure is called *homotopic marking* and its output is sometimes referred to as the *homotopic kernel* of the input image. This can be achieved by performing a sequential homotopic thinning until idempotence with the structuring element $\mathbf{D}$ shown in table 5.2. By doing so, simply connected components are reduced to a unique pixel and components containing holes to an equivalent number of 1-pixel thick closed loops.

5.5.3 Order independent homotopic thinnings

We first show that the homotopic marking of a set can be achieved by iterating order independent homotopic thinnings performed until stability. We then detail the notion of anchored skeletons allowing for more shape information to be preserved. An application to the extraction of crest lines on digital elevation models is finally presented.

Homotopic marking. By deleting order independent simple pixels until idempotence, a homotopic skeleton of the input image is produced without requiring the choice of a family of homotopic structuring elements. Indeed, this approach allows for all homotopic structuring elements to be considered simultaneously. In addition, the procedure is parallel and therefore independent of the order used for processing the image pixels. However, because *all*

possible homotopic SEs are taken into account, it generates an order independent homotopic marking of the input image rather than a skeleton preserving additional useful shape information. An example is shown in Fig. 5.16a on a series of characters extracted from plate numbers. As illustrated by the E and 2 characters, the order independent homotopic marking does not necessarily reduce simply connected sets to a single pixel. This is because such a reduction may be order dependent. For the same reason, closed loops appearing in the order independent homotopic marking of non-simply connected sets may have a thickness larger than 1 pixel. This occurs for all non-simply connected characters displayed in Fig. 5.16a.

Anchored skeleton. Usually, a homotopic marking is not preserving enough information about the shape of the input pattern. A solution to this problem is to predefine a set of pixels that should belong to the skeleton. By definition, these pixels are non-deletable and cannot be thinned when performing homotopic thinnings until idempotence. It follows that the resulting skeleton is anchored to these predefined pixels. They are therefore called *anchor points*. A classical set of anchor points consists of the centres of maximal discs or, equivalently, the skeleton by opening. This ensures that the obtained skeleton is suited for the reconstruction of the original image. When processing a binary set, the anchor points should be selected in accordance with the connectivity used for the foreground pixel. For instance, if the foreground is $\mathcal{G}$-connected, the elementary SE defined by $\overline{N}_{\mathcal{G}'}$ should be considered for computing the skeleton by opening according to Eq. 5.17. The resulting skeleton by opening corresponds to the $\mathcal{G}'$-connected local maxima of the distance function $D_{\mathcal{G}'}$. Figure 5.16b shows anchored skeletons of our set of characters using these local maxima as anchor points. In this figure, 8-connectivity is used for the foreground and therefore the anchor points are defined as the 4-connected local maxima of the city-block distance function D_4.

The skeleton gets a simpler structure by using the ultimate eroded set or, equivalently, the regional maxima[6] of the distance function $D_{\mathcal{G}'}$ as anchor points. Indeed, these anchor points are a subset of the local maxima of the distance function $D_{\mathcal{G}'}$. Anchored skeletons using the regional maxima of the distance function as anchor points are called *minimal skeletons*. Figure 5.16c shows the minimal skeletons of our set of characters. In both cases, each CC_8^1 of the original image contains at least one anchor point. Consequently, the order independent thinning does not change this property, i.e., it holds for all CC_8^1 of all subsequent thinned images. This is an important remark because the 8-deletability test can be skipped in situations where each CC_8^1 of the original image contains at least one anchor point: if a simple pixel p is in one of the four final configurations of Fig. 5.11, we are sure that it will be removed by all scanning orders.

[6] A regional maximum of an image is defined as a $\mathcal{G}^h$-connected component of pixels such that all its external boundary pixels have an elevation strictly lower than h.

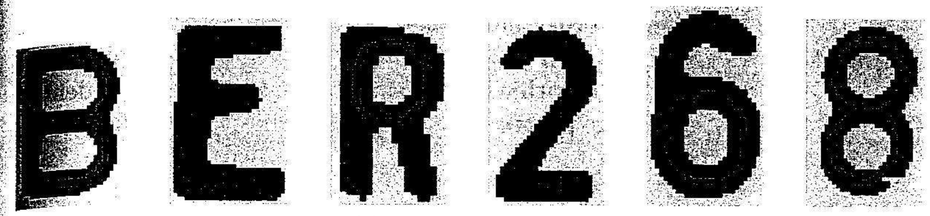

(a) Homotopic marking.

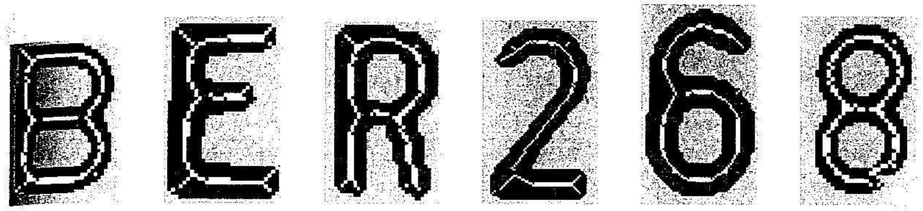

(b) Anchored skeleton using the 4-connected local maxima of D_4 as anchor points.

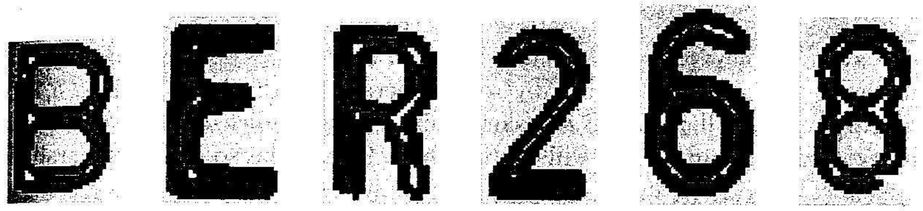

(c) Minimal skeleton (i.e., using the regional 4-connected maxima of D_4 as anchor points).

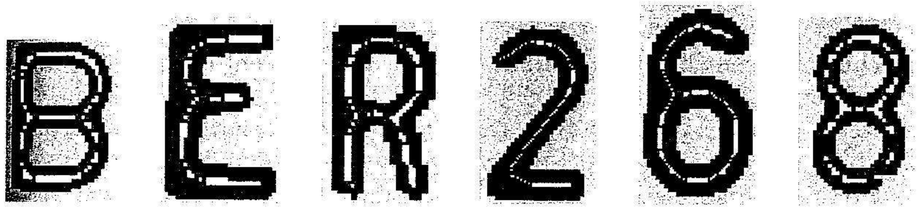

(d) Anchored skeleton using the 8-connected local maxima ≥ 4 of D_4 as anchor points.

Fig. 5.16. Skeletons of binary 8-connected characters based on order independent homotopic thinning schemes. Pixels of the skeleton are displayed in black and white (the latter defining the anchor points).

The minimal skeleton may remove too many skeletal branches (this happens for instance for the E, R, and 2 characters in Fig. 5.16c). Consequently, a trade-off between a skeleton allowing for reconstruction (possibly containing too many branches) and a minimal skeleton (possibly missing some relevant branches) is desirable in practice. This can be achieved by choosing intermediate anchor points, the selection criterion being application dependent. For example, by defining the anchor points as the 8-connected local maxima whose distance values in D_4 are greater or equal to 4, an acceptable skeletonisation of the characters is obtained as shown in Fig. 5.16d.

Note that when using order independent homotopic thinnings, the resulting skeletons are not as thin as those generated by homotopic sequential thinnings. Indeed, a given algorithm cannot simultaneously be independent of the order in which pixels are processed and lead to a one-pixel thick skeleton (incompatible properties).

Application. A practical application of grey tone skeletonisation is illustrated in Fig. 5.17. The input image shown in Fig. 5.17a represents a shaded view of a digital elevation model. Figure 5.17b depicts the grey tone order independent homotopic[7] skeleton of the input digital elevation model. It highlights the crest lines of the original image. This skeleton is in fact an order independent homotopic marking because no pre-defined anchor points have been used. That is, the network of crest lines is automatically anchored to the order independent homotopic thinning of the regional maxima of the input image. Predefined anchor points can also be used. If these anchor points are selected so that each CC_8^1 of each cross-section of the image contains at least one anchor point, the 8-deletability test can be skipped (similarly to binary images). The support of the grey tone skeletal lines displayed in Fig. 5.17c corresponds to all pixels of the skeletonised image which do not belong to a regional minimum[8]. We will see in Chap. 9 that the so-called watershed transformation is directly linked to grey tone skeletonisation in the sense that watersheds are a subset of the support of the grey tone skeleton. This is already highlighted by Fig. 5.17d which represents a labelling of the regional minima of the grey scale skeleton, i.e., each labelled region corresponds to a catchment basin while the crest lines located at catchment boundaries match the watersheds of the input image. Similarly to what happens for binary images, skeletal lines of a grey tone skeleton are not necessarily one pixel thick and may be in fact much thicker than 2 pixels (the maximal thickness is only limited by the size of the image). This is due to particular configurations of the grey scale values such as that illustrated in Fig. 5.18 and which has been sampled from Fig. 5.17b in a region where thick skeletal lines occur. The order independent thinning has set a thick region to the elevation 307. However, this thick region, although mostly surrounded by crest lines, cannot be further thinned (i.e., set to either 1 or 3 in this example) because it is itself leading to a crest line. That is, the pixel appearing in a shaded box is not simple (it matches the last neighbourhood configuration of the fourth row in Fig. 5.10). We will see that thick watershed zones (in the sense that one cannot decide whether the thick region drains to a catchment basin or another) always correspond to thick regions of the grey tone skeleton.

[7] In the sense of the cross-section topology introduced on page 56.

[8] A regional minimum of an image is defined as a $\mathcal{G}^h$-connected component of pixels such that all its external boundary pixels have an elevation strictly greater than h.

(a) Shaded view of a 1 km resolution digital elevation model (DEM) of the Pyrenean Alps (441 × 591 pixels).

(b) Grey scale skeleton by order homotopic thinning without anchor points, i.e., grey tone homotopic marking.

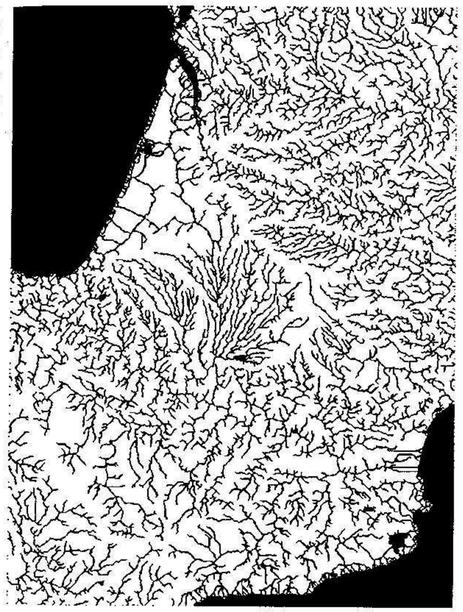

(c) Support of the skeletal lines.

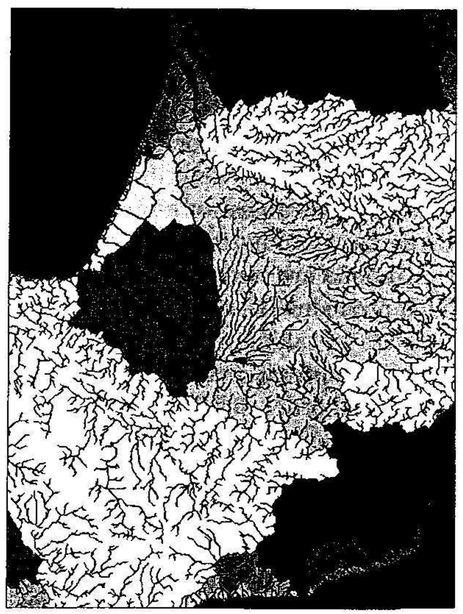

(d) Labelled regional minima of *(c)* whose closed loops delineate the catchment basins of the input DEM.

Fig. 5.17. Grey tone order independent homotopic skeletonisation without anchor points, i.e., homotopic marking.

3	3	3	3	3	3	3	3	3	3	3	3	3	3	3
3	3	3	3	3	3	611	3	3	3	3	3	3	3	3
3	3	3	3	3	3	530	3	3	3	3	3	3	3	3
3	3	3	705	3	3	584	3	3	3	3	3	478	3	3
3	3	3	639	584	584	584	760	423	423	423	3	423	428	434
3	3	3	651	307	307	307	307	307	423	307	423	3	3	3
3	3	632	307	307	307	307	307	307	307	307	307	**307**	3	3
705	3	632	307	362	362	362	362	362	362	362	370	1	**307**	3
2	705	705	362	1	1	1	1	1	1	1	1	1	1	329
2	2	705	830	823	1	1	1	1	1	1	1	1	1	1
2	2	2	2	2	859	606	1	1	1	1	1	1	1	1

Fig. 5.18. Thick skeletal lines extracted from Fig. 5.17b. The pixels at intensity 1, 2, and 3 belong to the regional minima of the grey tone skeleton, all other pixels belonging to the skeletal lines. The two pixels marked in bold clearly belong to the crest lines, impeding thereby further order independent homotopic thinning of the thick region.

5.5.4 Distance function

Another approach for skeletonising discrete sets consists in first computing a discrete distance function of the set and then process it so as to extract the skeleton of the original set (remember that the distance function mimics the wave front propagation).

Usually, some specific points of the distance function are detected and then used as anchor points. Classical points are the local and regional maxima, the latter leading to minimal skeletons. Note that the local maxima match the centre of maximal discs only when the distance function is discrete (i.e., either D_4 or D_8 in the square grid). In addition, contrary to the anchored skeleton described in the previous section, anchor points can be selected on any distance function because the distance values themselves are taken into account during the skeletonisation process. Indeed, the selected anchor points are connected by following the crest-lines of the distance function. This procedure is sometimes called 'upstream generation'. Another approach consists in taking into account the anchor points when performing distance order homotopic peeling of the set (i.e., all simple pixels are removed in a sequential order defined by the successive distance levels in order to mitigate the order dependence). Alternatively, full order independence can be achieved by computing the order independent skeleton of the distance function with the selected anchor points. This latter approach is illustrated in Fig. 5.19. The input image is a binary mask of the separation of the Rhône river in Arles (F) into the 'Petit' and 'Grand' Rhône rivers. This mask has been obtained by processing a Landsat image. We aim at extracting the medial line of the rivers. The rounded Euclidean distance transformation of this mask is shown in Fig. 5.19a. We define the anchor points shown in Fig. 5.19b as the regional maxima of the distance map having a value larger than 3. We finally compute the order independent skeletonisation of the distance transform with the previously described anchor points. The support of this grey

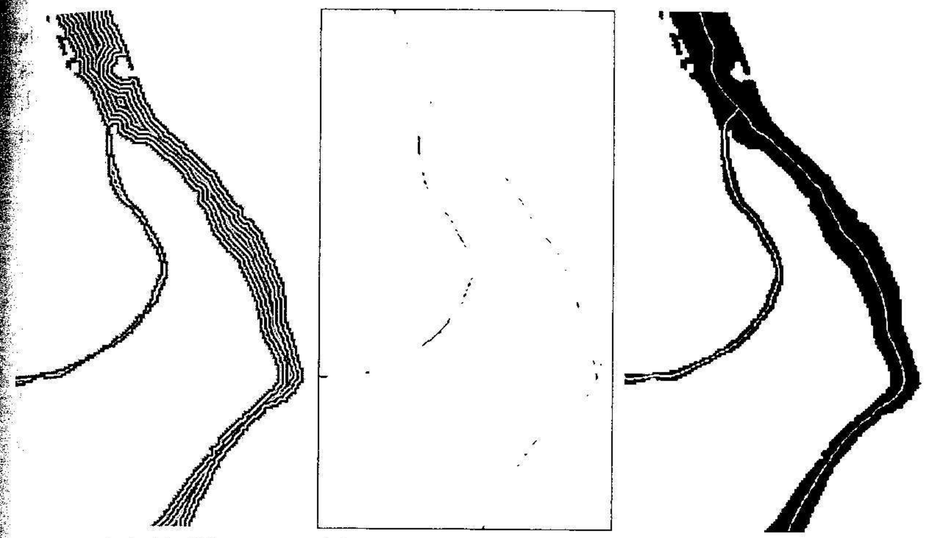

(a) Rounded Euclidean distance transform of an input river mask (351 × 476 image).

(b) Anchor points defined as the regional maxima of *(a)* with a distance larger than 3.

(c) Support of the skeletal lines of the grey tone anchored skeleton overlaid on input.

Fig. 5.19. Extraction of the medial line of a river network using grey tone anchored skeleton on a Euclidean distance transform of the rivers.

tone anchored skeleton is shown in Fig. 5.19c superimposed on the input river mask.

5.5.5 Skeleton pruning

Pruning is a transformation that iteratively removes the endpoints of an image either until stability or after a given number of iterations is reached. In this latter case, it can be used to shorten all skeletal branches of a skeleton while filtering out all branches shorter than the considered number of iterations.

The non-parametric pruning is implemented by detecting endpoints and by removing them until idempotence:

$$\mathrm{PRUNE}(X) = (X \underline{\circ} \mathbf{E})^{(\infty)}, \tag{5.20}$$

where the letter **E** refers to the SE used for detecting endpoints and ∞ indicates that the sequential thinning is iterated until stability. A parametric pruning of a given size n consists in removing n pixels of each branch of the skeleton, starting from each endpoint:

$$\mathrm{PRUNE}^{(n)}(X) = (X \underline{\circ} \mathbf{E})^{(n)}. \tag{5.21}$$

Parametric and non-parametric pruning of a skeleton are illustrated in Fig. 5.20. After a pruning of size 20 (Fig. 5.20b), all pixels belonging to

a chain of the skeleton and lying within a distance of less than 20 pixels from an endpoint are removed. By definition, the pruning of a skeleton as per Eqs. 5.20 and 5.21 requires a 1 pixel thick skeleton as input to proceed. When pruning until idempotence (Fig. 5.20c), the only parts of the skeleton that are not suppressed are the closed arcs or loops of the skeleton[9].

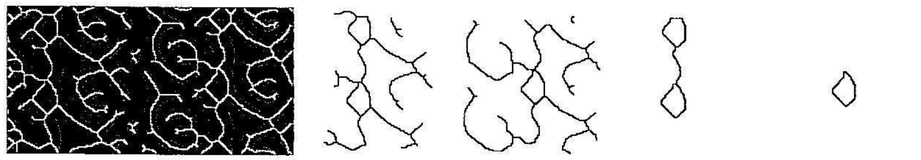

(a) Skeleton superimposed on the original set.

(b) The skeleton after pruning of size 20.

(c) Pruned skeleton (i.e., pruned until idempotence).

Fig. 5.20. Pruning of a skeleton: parametric in *(b)* and non-parametric in *(c)*.

Note that an alternative algorithm for obtaining the minimal skeleton of a set is to prune the original skeleton until points of the ultimate eroded set are encountered.

5.5.6 Skeleton by influence zones

The set of pixels of a binary image that are closer to a given connected component than any other connected component defines the influence zone of the considered connected component. There is therefore a one-to-one correspondence between the set of connected components of a binary image and the set of its influence zones. The boundaries of the influence zones define the skeleton by influence zones. An illustrative example is shown in Fig. 5.21.

In mathematical terms, let X be a binary image or set and $K_1, K_2, \ldots, K_n$ the connected components of X:

$$X = \bigcup_{i=1}^{n} K_i, \quad i \neq j \Rightarrow K_i \cap K_j = \emptyset. \tag{5.22}$$

The influence zone IZ of a particle K_i is the set of pixels of the image plane which is closer to K_i than any other particle of X:

$$\mathrm{IZ}(K_i) = \{p \mid \forall j \in \{1, \ldots, n\}, i \neq j \Rightarrow d(p, K_i) < d(p, K_j)\}. \tag{5.23}$$

In practice, the image of the influence zones IZ of a binary image is represented as a label image whereby each labelled region corresponds to the influence zone of a connected component of the input binary image.

[9] In discrete images, it may be that some multiple points remain after a pruning. This happens for instance when 3 lines oriented 60^o apart intersect on a unique point in the hexagonal graph. It is therefore necessary to skeletonise the remaining points and then repeat the whole procedure until stability.

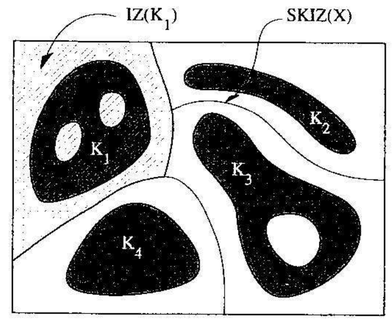

Fig. 5.21. Skeleton by influence zones (SKIZ) and associated influence zones (IZ) of a set X composed of four connected components $K_1, \ldots, K_4$. The hatched region highlights the influence zone of K_1.

The skeleton by influence zones or SKIZ is defined as the points that do not belong to any influence zone:

$$\mathrm{SKIZ}(X) = \complement \bigcup_{i} \mathrm{IZ}(K_i).$$

It is equivalent to the boundaries of the influence zones. When the input image consists of a collection of points, the resulting influence zones are known as the Voronoi polygons. The adjacency graph of the polygons is called a Delaunay triangulation, i.e., each vertex corresponds to a Voronoi polygon and two vertices are linked by an edge if the corresponding polygons are adjacent. When processing discrete images, the shape of the influence zones depends on the metric that is used for computing the distances in Eq. 5.23.

The SKIZ of a set is a subset of the pruned skeleton of the complement of this set:

$$\mathrm{SKIZ}(X) \subseteq \mathrm{PRUNE}[\mathrm{SK}(X^c)].$$

The skeleton of the complement of a set is sometimes called *exoskeleton* of X.

As exemplified in Fig. 5.22, digital SKIZ can be approximated by thickenings iterated until idempotence:

$$\mathrm{SKIZ}(X) = \{[(X \bigcirc \mathbf{L}^c)^{(\infty)} \bigcirc \mathbf{E}^c]^{(\infty)}\}^{(\infty)}.$$

In this equation, the sequence of sequential thickening performed until stability is itself iterated until stability. This illustrates the fact that the composition of two idempotent transformations is not necessarily an idempotent transformation.

A better approach for determining the SKIZ of a set consists in computing the watershed lines of the distance function on the complement of X:

$$\mathrm{SKIZ}(X) = \mathrm{WS}[D(X^c)], \tag{5.24}$$

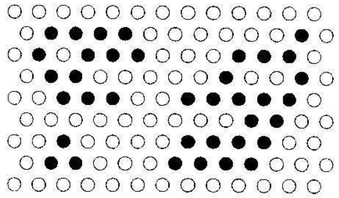

Binary image X.

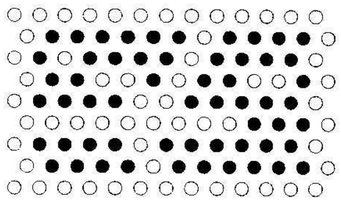

After thickening with $\mathbf{L}^c$ and its rotations until stability: $Y = (X \underline{\bigcirc} \mathbf{L}^c)^{(\infty)}$.

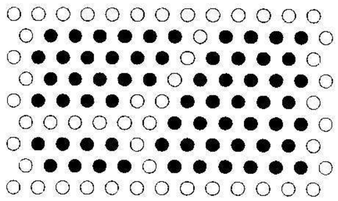

After thickening with $\mathbf{E}^c$ and its rotations until stability: $Z = (Y \underline{\bigcirc} \mathbf{E}^c)^{(\infty)}$.

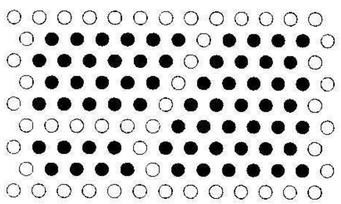

Final SKIZ:
$\mathrm{SKIZ}(X) = \{[(X \underline{\bigcirc} \mathbf{L}^c)^{(\infty)} \underline{\bigcirc} \mathbf{E}^c]^{(\infty)}\}^{(\infty)}$.

Fig. 5.22. Skeleton by influence zones by thickenings. Thickenings with $\mathbf{L}^c$ and its rotations output a $\mathbf{L}$-skeleton of the background of the image (exoskeleton). This skeleton is then pruned with the SE $\mathbf{E}^c$. The SKIZ is obtained by iterating these two steps until idempotence.

where WS denotes the watershed transformation (see Chap. 9, Sec. 9.2.2). Accordingly, the influences zones of a binary image X correspond to the catchment basins CB of the distance function on the complement of X:

$$\mathrm{IZ}(X) = \mathrm{CB}[D(X^c)].$$

The properties of all presented discrete skeletons are summarised in table 5.3. Skeletons in terms of maximal discs and openings are identical for binary images but the latter definition is suited to the processing of grey tone images. All six definitions can be extended to the processing of 3-D images.

Table 5.3. Some properties of the presented discrete skeletons. The column 'Reconstruction' indicates whether the output skeleton enables the reconstruction of an input binary set while the column 'Grey' tells whether the methodology is applicable to grey tone images.

Definition in terms of	Homotopic	Reconstruction	Grey	Order independence	Thickness
Openings (Eq. 5.17)	no	yes	yes	yes	≥ 1
Maximal discs (Eq. 5.18)	no	yes	no	yes	≥ 1
Seq. homotopic thinnings (Eq. 5.19)	yes	no	yes	no	1
Order indep. homotopic thinnings	yes	yes[a]	yes	yes	≥ 1
Dist funct. + upstream generation	yes	yes	no	yes	≥ 1
Influence zones	no	no	yes	–[b]	–[b]

[a] Provided that anchor points allowing for reconstruction are used.
[b] Depends on the implementation.

Note that if the considered algorithm outputs thick skeletal lines (e.g., due to the considered anchor points or an order independent scheme), the resulting skeleton can always be thinned by an additional (order dependent) thinning step. This may be required by skeleton post-processing such as the pruning of noisy branches. By doing so, order dependent decisions are only taken at the very latest step.

5.5.7 Two practical applications

In this section, we detail two additional practical applications based on a skeletonisation procedure. They concern the separation of crossing fibres and the extraction of grid lines on industrial metal sheets.

Separation of overlapping fibres. In some applications, there is need to separate elongated objects that intersect each other. For example, Fig. 5.23a represents three fibres that are crossing each other. A solution to this problem consists in first computing the skeleton of the input image (Fig. 5.23b). Each intersection between two fibres generates multiple points in their skeleton representation but there are also additional multiple points due to small skeletal branches. These latter branches are removed using a parametric pruning (Fig. 5.23c). The remaining multiple points are then dilated (Fig. 5.23d)

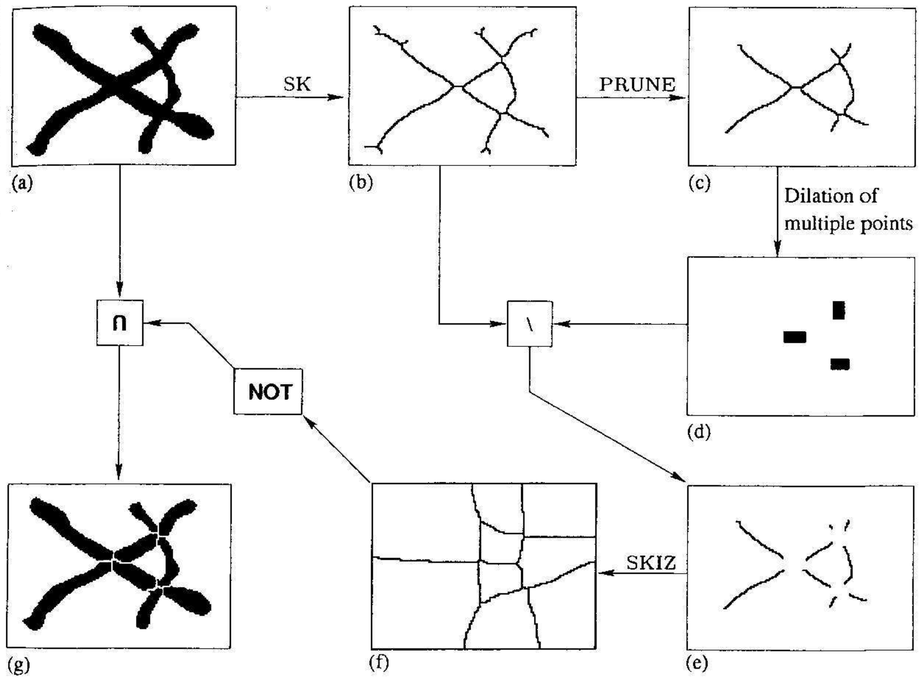

Fig. 5.23. Use of skeletonisation for separating overlapping fibres.

and suppressed from the skeleton (Fig. 5.23e). The dilation allows us to merge multiple points that lie close to each other. Indeed, the skeleton of the intersection of two thick fibres usually generates two rather than a unique multiple point. The skeleton by influence zones of the remaining skeleton is then computed (Fig. 5.23f). Finally, the skeletal lines which lie within the original fibres separate the fibres (Fig. 5.23g).

Grid node extraction. Another application of skeletons is presented in Fig. 5.24. It concerns the final steps for the extraction of grid nodes on metallic surfaces, see Sec. 4.7. In this latter section, we have shown how to obtain a mask of the grid lines. This mask is now skeletonised and pruned until idempotence. The resulting skeleton contains some irrelevant branches that are filtered using a size criterion: components of the background of the skeleton that are smaller than a given threshold value are removed. The multiple points of the resulting filtered skeleton correspond to the grid nodes of the original image. Figure 5.25 illustrates the same methodology applied to another image.

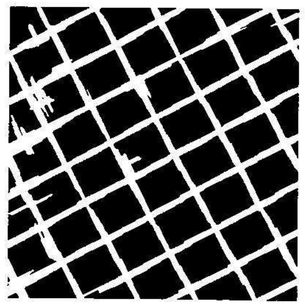

Mask of grid lines

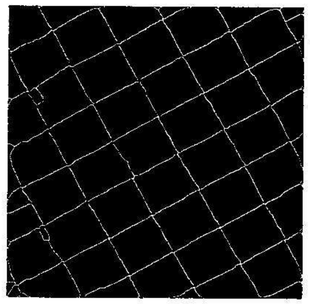

Pruned skeleton of grid lines

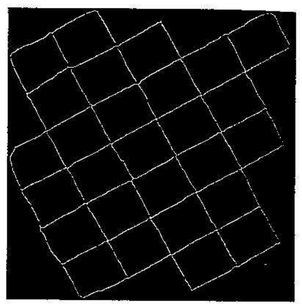

Filtered skeleton

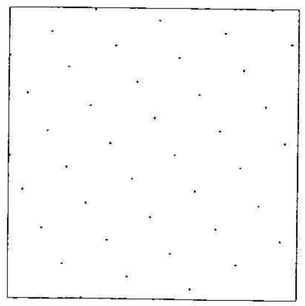

Grid nodes extracted from the filtered skeleton

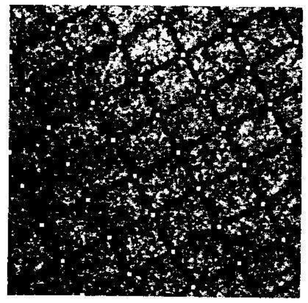

Grid nodes superimposed on original image

Fig. 5.24. Use of skeletons for extracting the intersection points of a set of thick grid lines drawn on sheet steel.

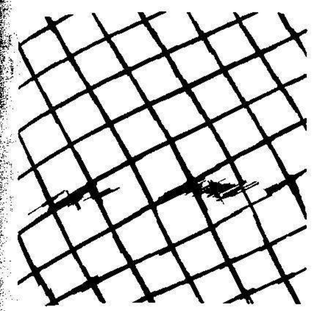

Mask of grid lines.

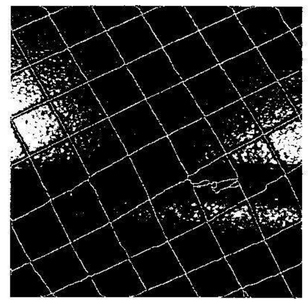

Pruned skeleton of grid lines on input image.

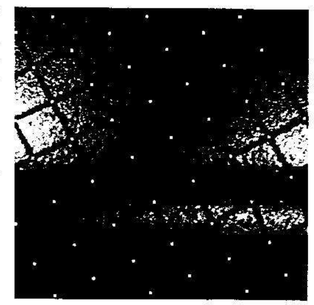

Final grid nodes.

Fig. 5.25. Another example for the extraction of grid lines (Peyrard et al., 1995).

5.6 Computation of HMTs and skeletons

We first detail a generic algorithm for computing the hit-or-miss transformation for binary images and then briefly describe some skeletonisation algorithms.

5.6.1 Look-up-table implementation of binary HMTs

The computation of hit-or-miss transformations is not necessarily based on an intersection of two erosions, i.e., as per Eq. 5.2. A search for a specific configuration can be done directly by using a look-up-table (LUT). Let $\{p_0, p_1, \ldots, p_n\}$ be the set of pixels of a composite structuring element $\mathbf{B}$, its origin being at p_0. The coding function CF of $\mathbf{B}$ is then defined as follows:

$$\mathrm{CF}(\mathbf{B}) = \sum_{i=0}^{n} 2^i k(p_i), \tag{5.25}$$

where $k(p_i)$ is the indicator function of p_i:

$$k(p_i) = \begin{cases} 1, \text{ if } p_i \in B_{\mathrm{FG}}, \\ 0, \text{ if } p_i \in B_{\mathrm{BG}}. \end{cases} \tag{5.26}$$

A unique code corresponds therefore to each composite SE defined on the pixels $p_0, p_1, \ldots, p_n$, the origin being at p_0. An example is provided in Fig. 5.26. The coding CF of each pixel p of a binary image f is then computed as follows:

$$\mathrm{CF}(p) = \sum_{i=0}^{n} 2^i f(p_i), \tag{5.27}$$

where the origin p_0 of the considered SE matches p. The hit-or-miss transform HMT of the binary image f by the SE $\mathbf{B}$ is then calculated as follows:

Fig. 5.26. Coding of a composite structuring element defined on the elementary hexagon. *Left:* elementary hexagon and its pixels p_i. *Right:* composite structuring element $\mathbf{P}$ used for extracting non-isolated endpoints. The grey discs belong to P_1 and the white discs belong to P_2. The coding function CF leads to the follow code: $\mathrm{CF}(\mathbf{P}) = 2^0 + 2^6 = 65$.

$$\left[\mathrm{HMT}_{\mathbf{B}}(f)\right](p) = \begin{cases} 1, & \text{if } \mathrm{CF}(p) = \mathrm{CF}(\mathbf{B}), \\ 0, & \text{otherwise.} \end{cases} \tag{5.28}$$

If rotation invariance is needed, a HMT is performed for the n possible rotations Θ of the structuring element $\mathbf{B}$:

$$\bigcup_{i=1}^{n} \mathrm{HMT}_{\Theta_i \mathbf{B}}(f). \tag{5.29}$$

The implementation using a LUT proceeds as follows. First a LUT of size equal to 2^n where n is the number of pixels of the composite SE is created. An element at position index i of this array is initialised to one if this position index corresponds to the coded value of a SE, otherwise it is set to zero. The LUT allows us to compute in parallel the hit-or-miss transform with all coded SEs:

$$\bigcup_{i=1}^{n} \left[\mathrm{HMT}_{\Theta_i \mathbf{B}}(f)\right](p) = \begin{cases} 1, & \text{if } \exists i \in [1,n],\ \mathrm{LUT}[\mathrm{CF}(p)] = 1. \\ 0, & \text{otherwise.} \end{cases} \tag{5.30}$$

For instance, the codes of the structuring element $\mathbf{P}$ shown in Fig. 5.26 and its 5 successive counterclockwise rotations by 60^o are 65, 3, 5, 9, 17, and 33. These codes permit the extraction of all non-isolated endpoints on a hexagonal graph, whatever their orientation.

The LUT implementation of the hit-or-miss transform is limited by the size of the SE since the coding requires one bit per SE pixel. Hence, the direct implementation following Eq. 5.1 is usually required for SEs larger than those defined within the elementary neighbourhood of a pixel.

5.6.2 Skeletonisation algorithms

Following the lack of a clear and unique definition for the skeletonisation of a discrete set, many research reports have been devoted to the computation of skeletons. A survey about thinning-based skeletonisation algorithms including 138 references is provided in (Lam et al., 1992). Algorithms for producing

order independent binary and grey scale anchored skeletons are proposed by Ranwez and Soille (2002).

There are many papers devoted to the extraction of skeletons on the distance transforms of the binary set. For example, a one pass two-operation process to detect the skeletal pixels on the 4-distance transform has been proposed by Arcelli and Sanniti di Baja (1989).

Efficient computation of various types of skeletons based on homotopic peelings using the maxima of the distance function or the ultimate eroded set as anchor points are detailed in (Vincent, 1991) and extended to 3-D images by Pudney (1998). Fast homotopic peelings are possible thanks to a queue data structure and a look-up-table indicating whether a given configuration preserves the homotopy or not. This approach is extended to the computation of Euclidean skeletons in (Talbot and Vincent, 1992; Svensson et al., 1999). The thickness of the resulting skeletons may be of two pixels. An adaptation leading to one pixel thick skeletons is proposed in (Schmitt, 1994).

Digital approximations of Euclidean skeletons can be found in (Montanari, 1968) and (Meyer, 1990). Algorithms for skeletons of three-dimensional images are proposed in (Lobregt et al., 1980), (Borgefors et al., 1999), and (Jonker, 2002).

5.7 Bibliographical notes and references

Hit-or-miss transforms for binary images are extensively detailed in (Serra, 1982). This transform has the same effect as the *template matching* operator proposed in (Crimmins and Brown, 1985). Banon and Barrera (1991) have shown that any translation invariant mapping can be represented as a union of a family of hit-or-miss transformations. Table 5.4 summarises the representation theorems stated so far.

Table 5.4. Morphological representation of translation invariant mappings satisfying some additional properties.

Properties	Representation
Translation invariance (T.I.) only	Union of hit-or-miss (Sec. 5.7)
T.I. and increasing	Union of erosions (Sec. 3.10)
T.I., increasing, idempotent, and anti-extensive	Union of morphological openings (Sec. 4.4)

Note that the generalisations of the hit-or-miss transform for grey scale images presented in Sec. 5.1.2 depart from that proposed in (Serra, 1982, p. 450). The hit-or-miss opening introduced in Sec. 5.1.4 is called *generalised foreground opening* by Bloomberg and Maragos (1990) in the context of binary images where it is used for as a basic tool for character recognition. It is

also referred to as the *opening overcondensation* by Ronse (1996) in a thorough paper devoted to their properties (including representation theorems and rank based extensions) in the general framework of complete lattices.

The computation of the connectivity number (also called Euler characteristic) of binary images in the square and triangular grids is discussed in (Gray, 1971). This paper also presents the notion of *Euler differential*, i.e., the variation of the connectivity number of the binary neighbourhood $\overline{N}_{\mathcal{G}_{\max}}(p)$ occurring when changing the state of p from 1 to 0 or vice versa. Consequently, homotopic neighbourhood configurations are those whose Euler differential is null.

Constrained thinnings and thickenings have been extended to grey scale images by Goetcherian (1980) and Beucher (1981, 1990). The filtering of white (resp. black) noisy pixels in grey scale images using grey scale thinnings (resp. thickenings) with the SE I (resp. $\mathbf{I}^c$) for isolated pixels has also been proposed in (Goetcherian, 1980). The *Golay alphabet* has been introduced by Serra (1982) in reference to the work of Golay (1969) on hexagonal pattern transformations. The notion of unconstrained thinnings and thickenings are new developments following the definition of the unconstrained hit-or-miss for grey scale images.

The rank hit-or-miss transform is studied in (Casasent and Sturgill, 1990) (where they are called rank order hit-or-miss) and (Bloomberg and Maragos, 1990) (where they are called rank hit-miss transform). In fact, the concept of rank hit-or-miss transform goes back to the work of Wilson (1989) who generalised the inclusion conditions of the hit-or-miss transform to partial inclusion while allowing for an arbitrary number of input image components (rather than only X and X^c), the output value at a given pixel being itself defined by sorting the output of each component processed in parallel by a rank filter with structuring element B_i and rank k_i, and selecting a given rank k:

$$\zeta_k[\zeta_{B_1,k_1}(X_1),\ldots,\zeta_{B_n,k_n}(X_n)].$$

First applications dealt with optical character recognition tasks (Wilson, 1989). Complete systems for automatic target recognition are described in (Casasent and Sturgill, 1990). In this book, we have shown that all concepts apply to grey scale images.

Blum (1967, 1973) introduced the notions of medial axis and skeleton using the concept of grass-fire. The definition in terms of maximal discs has been proposed by Calabi and Hartnett (1968). Contrary to what happens with discrete distance functions, the centres of maximal discs cannot be extracted from a local neighbourhood when dealing with Euclidean distance transforms. This issue is addressed in (Ge and Fitzpatrick, 1996).

The definition of the Euclidean skeleton by opening is due to Lantuéjoul (1978). Its application to discrete images (Eq. 5.17) is suited to the processing of grey scale images as shown in (Peleg and Rosenfeld, 1981). This latter work is at the basis of the hierarchical (multiresolution) morphological image

decomposition scheme presented by Toet (1990) and applied to image filtering in (Vachier et al., 1994).

Topological properties of Euclidean skeletons have been extensively studied by Matheron (1988) and then transferred to discrete sets by Meyer (1988, 1989). The latter paper also defines the notions of upstream generation and minimal skeleton. Beucher (1994) has shown that there exists a link between skeletons by maximal discs and sequential thinnings. Note that thinning operators and skeletons are not restricted to the framework of morphology. An early reference on this topic is due to (Hilditch, 1969). References to algorithms for computing digital skeletons are given in Sec. 5.6.2.

The notion of deletable (also called simple) pixel is due to Rosenfeld (1970). Extensions to the 3-D cubic grid are proposed by Bertrand (1994) and Kong (1995). A topological characterisation of thinning including the notion of strong $\mathcal{G}$-deletability of a connected component of pixels is proposed by Ronse (1986). This idea is further developed in (Ronse, 1988) for characterising *parallel* homotopic thinnings. The advantage of parallel over sequential homotopic thinnings is that in the former case there is no need to choose a family of SEs nor an order for processing the image pixels. Similar ideas are at the basis of the notion of order independent homotopic thinning developed by Ranwez and Soille (1999, 2002). Bertrand et al. (1997) introduce the notion of lower and upper homotopic kernels of a grey tone image. The notion of grey tone homotopic marking originally presented in (Ranwez and Soille, 2002) corresponds to an *order independent* lower homotopic kernel.

Discrete and Euclidean skeletons by influence zones are studied in depth in (Lantuéjoul, 1978 & 1980). Finally, the use of skeletons for coding images is discussed in (Maragos and Schafer, 1986) and (Kresch and Malah, 1994).

C. Arcelli and G. Sanniti di Baja. A one pass two-operation process to detect the skeletal pixels on the 4-distance transform. *IEEE Transactions on Pattern Analysis and Machine Intelligence*, 11(4):411–414, April 1989.

G. Banon and J. Barrera. Minimal representation for translation-invariant set mappings by mathematical morphology. *SIAM Journal on Applied Mathematics*, 51:1782–1798, 1991.

G. Bertrand. Simple points, topological numbers and geodesic neighborhoods in cubic grids. *Pattern Recognition Letters*, 15:1003–1011, 1994.

G. Bertrand, J.-C. Everat, and M. Couprie. Image segmentation through operators based upon topology. *Journal of Electronic Imaging*, 6(4):395–405, 1997.

S. Beucher. Ligne de partage des eaux : comment l'expliquer en termes de transformation fonctionnelle ? Technical Report N-699, Ecole des Mines de Paris, May 1981.

S. Beucher. *Segmentation d'Images et Morphologie Mathématique*. PhD thesis, Ecole des Mines de Paris, June 1990.

S. Beucher. Digital skeletons in Euclidean and geodesic spaces. *Signal Processing*, 38(1):127–141, July 1994.

D. Bloomberg and P. Maragos. Generalized hit-miss operations. In P. Gader, editor, *Image Algebra and Morphological Image Processing*, volume SPIE-1350, pages 116–128, 1990.

H. Blum. A transformation for extracting new descriptors of shape. In W. Wathen-Dunn, editor, *Models for the Perception of Speech and Visual Form*, pages 362–380, Cambridge, MA, 1967. M.I.T. Press.

H. Blum. Biological shape and visual science (part 1). *Journal of Theoretical Biology*, 38:205–287, 1973.

G. Borgefors, I. Nyström, and G. Sanniti di Baja. Computing skeletons in three dimensions. *Pattern Recognition*, 32(7):1225–1236, 1999.

L. Calabi and W. E. Hartnett. Shape recognition, prairie fires, convex deficiencies and skeletons. *Amer. Math. Monthly*, 75:335–342, 1968.

D. Casasent and R. Sturgill. Optical hit-or-miss morphological transforms for ATR. In A. Tescher, editor, *Applications of Digital Image Processing XII*, volume SPIE-1153, pages 500–510, 1990.

T. Crimmins and W. Brown. Image algebra and automatic shape recognition. *IEEE Transactions on Aerospace and Electronic Systems*, 21(1):60–69, January 1985.

H. Freeman. Computer processing of line-drawing images. *Computing Surveys*, 6: 57–97, March 1974.

Y. Ge and J. Fitzpatrick. On the generation of skeletons from discrete Euclidean distance maps. *IEEE Transactions on Pattern Analysis and Machine Intelligence*, 18(11):1055–1066, November 1996.

V. Goetcherian. From binary to grey tone image processing using fuzzy logic concepts. *Pattern Recognition*, 12:7–15, 1980.

M. Golay. Hexagonal parallel pattern transformation. *IEEE Transactions on Computers*, 18(8):733–740, August 1969.

S. Gray. Local properties of binary images in two dimensions. *IEEE Transactions on Computers*, 20(5):551–561, May 1971.

C. Hilditch. Linear skeletons form square cupboards. In B. Mertzer and D. Michie, editors, *Machine Intelligence*, volume 4, chapter 22, pages 403–420. University Press, Edinburgh, 1969.

P. Jonker. Skeletons in N dimensions using shape primitives. *Pattern Recognition Letters*, 23(6):677–686, April 2002.

T. Kong. On topology preservation in 2-D and 3-D thinning. *International Journal of Pattern Recognition and Artificial Intelligence*, 9(5):813–844, 1995.

R. Kresch and D. Malah. Multi-parameter skeleton decomposition. In J. Serra and P. Soille, editors, *Mathematical Morphology and its Applications to Image Processing*, pages 141–148. Kluwer Academic Publishers, 1994.

L. Lam, S.-W. Lee, and C. Suen. Thinning methodologies: a comprehensive survey. *IEEE Transactions on Pattern Analysis and Machine Intelligence*, 14(9):869–885, 1992.

C. Lantuéjoul. *La Squelettisation et son Application aux Mesures Topologiques des Mosaïques Polycristallines*. PhD thesis, Ecole des Mines de Paris, 1978.

C. Lantuéjoul. Skeletonization in quantitative metallography. In R. Haralick and J.-C. Simon, editors, *Issues in Digital Image Processing*, volume 34 of *NATO ASI Series E*, pages 107–135, Alphen aan den Rijn, 1980. Sijthoff & Noordhoff.

S. Lobregt, P. Verbeek, and F. Groen. Three-dimensional skeletonization: principle and algorithm. *IEEE Transactions on Pattern Analysis and Machine Intelligence*, 11(1):75–77, January 1980.

P. Maragos and R. Schafer. Morphological skeletons representation and coding of binary images. *IEEE Transactions on Acoustics, Speech, and Signal Processing*, 34(5):1228–1244, October 1986.

M. Matheron. Examples of topological properties of skeletons. In J. Serra, editor, *Image Analysis and Mathematical Morphology. Volume 2: Theoretical Advances*, chapter 11, pages 217–238. Academic Press, 1988.

F. Meyer. Skeletons in digital spaces. In J. Serra, editor, *Image Analysis and Mathematical Morphology. Volume 2: Theoretical Advances*, chapter 13, pages 257–296. Academic Press, London, 1988.

F. Meyer. Skeletons and perceptual graphs. *Signal Processing*, 16:335–363, 1989.

F. Meyer. Digital Euclidean skeletons. In M. Kunt, editor, *Visual Communications and Image Processing'90*, volume SPIE-1360, pages 251–262, Lausanne, 1990. Society of Photo-Instrumentation Engineers.

U. Montanari. A method for obtaining skeletons using a quasi-Euclidean distance. *Journal of the ACM*, 15(4):600–624, October 1968.

S. Peleg and A. Rosenfeld. A min-max medial axis transform. *IEEE Transactions on Pattern Analysis and Machine Intelligence*, 3:208–210, March 1981.

R. Peyrard, P. Soille, J.-C. Klein, and A. Tuzikov. A dedicated hardware system for the extraction of grid patterns on stamped metal sheets. In I. Pitas, editor, *Proc. of 1995 IEEE Workshop on Nonlinear Signal and Image Processing*, pages 867–870, Neos Marmaras, June 1995.

C. Pudney. Distance-ordered homotopic thinning: a skeletonization algorithm for 3D digital images. *Computer Vision and Image Understanding*, 72(3):404–413, December 1998.

V. Ranwez and P. Soille. Order independent homotopic thinning. In G. Bertrand, M. Couprie, and L. Perroton, editors, *Proc. of Discrete Geometry for Computer Imagery'99*, volume 1568 of *Lecture Notes in Computer Science*, pages 337–346. Springer-Verlag, 1999.

V. Ranwez and P. Soille. Order independent homotopic thinning for binary and grey tone anchored skeletons. *Pattern Recognition Letters*, 23(6):687–702, April 2002.

C. Ronse. A topological characterization of thinning. *Theoretical Computer Science*, 43:31–41, 1986.

C. Ronse. Minimal test patterns for connectivity preservation in parallel thinning algorithms for binary digital images. *Discrete Applied Mathematics*, 21:67–79, 1988.

C. Ronse. A lattice-theoretical morphological view on template extraction in images. *Journal of Visual Communication and Image Representation*, 7(3):273–295, September 1996.

A. Rosenfeld. Connectivity in digital pictures. *Journal of the ACM*, 17(1):146–160, 1970.

M. Schmitt. One pixel thick skeletons. In J. Serra and P. Soille, editors, *Mathematical Morphology and its Applications to Image Processing*, pages 257–264. Kluwer Academic Publishers, 1994.

J. Serra. *Image Analysis and Mathematical Morphology*. Academic Press, London, 1982.

S. Svensson, G. Borgefors, and I. Nyström. On reversible skeletonization using anchor-points from distance transforms. *Journal of Visual Communication and Image Representation*, 10:379–397, 1999.

H. Talbot and L. Vincent. Euclidean skeletons and conditional bisectors. In P. Maragos, editor, *Visual Communications and Image Processing*, volume SPIE-1818, pages 862–876, 1992.

A. Toet. A hierarchical morphological image decomposition. *Pattern Recognition Letters*, 11:267–274, April 1990.

C. Vachier, F. Meyer, C. Gratin, and H. Talbot. Filtrage par décomposition morphologique : application à l'extraction de structures rectilignes. In *Reconnaissance des Formes et Intelligence Artificielle*, pages 255–263, Paris, 1994. GRETSI.

L. Vincent. Efficient computation of various types of skeletons. In M. Loew, editor, *Medical Imaging V: Image Processing*, volume SPIE-1445, pages 297–311, 1991.

S. Wilson. Vector morphology and iconic neural networks. *IEEE Transactions on Systems, Man, and Cybernetics*, 19(6):1636–1644, 1989.

6. Geodesic Transformations

All morphological transformations discussed so far involved combinations of *one* input image with specific structuring elements. The approach taken with geodesic transformations is to consider *two* input images. A morphological transformation is applied to the first image and it is then forced to remain either above or below the second image. Authorised morphological transformations are restricted to elementary erosions and dilations. The choice of specific structuring elements is therefore eluded. In practice, geodesic transformations are iterated until stability making the choice of a size unnecessary. It is actually the combination of appropriate pairs of input images which produces new morphological primitives. These primitives are at the basis of formal definitions of many important image structures for both binary and grey scale images.

The chapter is organised as follows. Elementary geodesic operators are introduced in Sec. 6.1. The iteration of these operators converges after a finite number of iterations. This leads to the definition of morphological reconstruction algorithms detailed in Sec. 6.2. Morphological primitives based on morphological reconstruction are reviewed in Sec. 6.3. A practical application dealing with the interpolation of contour data is presented in Sec. 6.4. Bibliographical notes and references are provided in Sec. 6.5.

An alternative approach to geodesic morphology stems from the concept of geodesic distance. The associated metric and related transformations are the scope of Chap. 7.

6.1 Elementary geodesic transformations

We first define the geodesic dilation and the dual geodesic erosion. We then show how to construct a self-dual geodesic transformation by combining these two operations.

6.1.1 Geodesic dilation

A geodesic dilation involves two images: a marker image and a mask image. By definition, both images must have the same definition domain and the